

SECOND QUARTERLY PROGRESS REPORT

on

DEVELOPMENT OF LARGE-INTERNAL-SURFACE-AREA
NICKEL METAL PLAQUES

(Period Covered: September 18 through December 18, 1964)

January 15, 1965

by

J. McCallum, G. R. Schaer, D. G. Trevethan, and C. L. Faust

Contract NAS 3-6003

Prepared for

NASA-LEWIS RESEARCH CENTER
SPACE POWER SYSTEMS DIVISION

Technical Manager
Mr. W. A. Robertson
MS500-201

BATTELLE MEMORIAL INSTITUTE
505 King Avenue
Columbus, Ohio 43201
Telephone: Area Code 614 299:3151

Battelle Memorial Institute • COLUMBUS LABORATORIES

505 KING AVENUE COLUMBUS, OHIO 43201 • AREA CODE 614, TELEPHONE 299-3151 • CABLE ADDRESS: BATMIN

February 16, 1965

National Aeronautics and Space Administration
Lewis Research Center
Space Power Systems Procurement Section
21000 Brookpark Road
Cleveland, Ohio 44135

Attention John E. Dilley, MS 500-309
Contracting Officer

Second Quarterly Progress Report
"Development of Large-Internal-Surface Area
Nickel Metal Plaques"
Contract NAS 3-6003

This is your copy of the Second Quarterly Progress Report on Contract NAS 3-6003. It covers the period between September 18 and December 18, 1964. A rough draft of this report was mailed on January 15, 1965, to Mr. William A. Robertson for his review as Technical Project Manager for your organization.

Distribution of the report is being made in accordance with Article II-B, paragraph 2, of the contract. Past reports mailed to the following addresses were returned to us unclaimed:

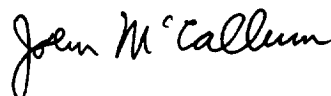
Capt. William H. Ritchie
Space Systems Division
Attention: SSZAE-11
Air Force Unit Post Office
Los Angeles 45, California

Capt. William Hoover
Air Force Ballistic Missile Division
Attention: WEZYA-21
Air Force Unit Post Office
Los Angeles 45, California

Consequently their names are being deleted from the mailing list that was in the First Quarterly Progress Report.

Comments about the reported work are welcome.

Yours sincerely,



John McCallum
Project Leader

JM:pa
Enc.

TABLE OF CONTENTS

	<u>Page</u>
INTRODUCTION AND OBJECTIVES	1
SUMMARY	2
FUTURE WORK	3
EXPERIMENTAL WORK BY TASKS	3
Task A - Raw Material Classification	3
Task B - Porous Mat Manufacture	4
Objectives	4
Item 1 - Thickness Range	4
Item 2 - Techniques for Making Mats	4
Stacking Screens	4
Electroforming Screens	5
Item 3 - Methods for Controlling Pore Shapes	9
Control of Porosity	9
Future Work	11
Location of Data	12
Task C - Sintered-Plaque Processing	12
Task D - Plaque Classification	12
Task E - Impregnation Procedure	13
Objectives	13
Physical Packing Methods	13
Cadmium Metal Powder	13
Cadmium Oxide	13
Cadmium Hydroxide	14
Future Work	14
Location of Data	14
Task F - Electrochemical Evaluation	14
Objectives	14
Item 1 - Energy Output	14
Relationship of Cell Components to Commercial Cells	15
Weight and Size Breakdown	15
Reproducibility	16
Effect of Flooding	17
Energy-Conversion Factors	17
Commercial Single Positive Electrodes	19
Effect of Rate of Discharge	19
Oxygen Effect	20
Commercial Single Negative Electrodes	20
Chemical Analysis	20
Experimental Methods	25
Effect of Rate of Discharge	25
Hydrogen Effect	27
Cycling Effect	27

TABLE OF CONTENTS (Continued)

	<u>Page</u>
N/P Ratios	32
Energy-Conversion Factors	34
Step 1 - Theoretical	34
Step 2 - Electrochemical	34
Step 3 - Cycle	35
Step 4 - Overall	35
Experimental Screen Electrodes	35
Effect of Pore Size	35
Energy Input	37
Commercial Standard Electrodes	37
Effects of Current Density	37
Future Work	40
Location of Data	40

LIST OF FIGURES

Figure 1.	Top Surface of Superimposed 250-Mesh Screens Before Bonding . .	6
Figure 2.	Top Surface of Superimposed 250-Mesh Screens Before Bonding . .	6
Figure 3.	Top Surface of Superimposed 250-Mesh Screens After Bonding . .	6
Figure 4.	Bottom Surface of Superimposed 250-Mesh Screens After Bonding . .	6
Figure 5.	Top Surface of Superimposed 250-Mesh Screens Before Bonding . .	7
Figure 6.	Top Surface of Superimposed 250-Mesh Screens After Bonding . .	7
Figure 7.	Bottom Surface of Superimposed 250-Mesh Screens After Bonding . .	7
Figure 8.	Top Surface of Superimposed 500-Mesh Screens Before Bonding . .	7
Figure 9.	Top Surface of Superimposed 500-Mesh Screens After Bonding . .	8
Figure 10.	Bottom Surface of Superimposed 500-Mesh Screens After Bonding . .	8
Figure 11.	Surface View of Stacked and Bonded 250-Mesh Screens - Semi- Random Orientation	9
Figure 12.	Half-Cell Discharge Data From Commercial Nickel-Cadmium Electrodes	21
Figure 13.	Half-Cell Discharge Data From Commercial Nickel-Cadmium Electrodes	22
Figure 14.	Average Voltage of Positive Half-Cell Vs Current Density	23

LIST OF FIGURES (Continued)

	<u>Page</u>
Figure 15. Capacity of Negative Plates as a Function of Charge-Discharge Cycles	28
Figure 16. Cross Section of a Commercial Impregnated Battery Plate Before Cycling (Without Overlay)	30
Figure 17. Cross Section of a Commercial Impregnated Battery Plate Before Cycling (With Overlay)	30
Figure 18. Cross Section of a Commercial Impregnated Battery Plate After Five Charge-Discharge Cycles of 100 Percent Depth	31
Figure 19. Cross Section of Battelle Impregnated Commercial Sintered Nickel Plate After Five Charge-Discharge Cycles of 100 Percent Depth	31
Figure 20. Capacity of Negative Plates as a Function of Charge-Discharge Cycles	36
Figure 21. Charge Curve for Negative Electrode at a Current Density of 9.65 ma/cm ²	38
Figure 22. Coulombic Input to Evolve Hydrogen as a Function of Charging-Current Density	39

LIST OF TABLES

Table 1. Relationship of Hole Size and Porosity of Screens	10
Table 2. Nickel Etching Rates in Ferric Chloride Solutions	11
Table 3. Physical Dimensions for Separate Components of a Commercial Nickel-Cadmium Cell	15
Table 4. Effect of Flooding in a Commercial Nickel-Cadmium Cell	17
Table 5. Approximate Weight and Volume Factors for Estimating Performances From Individual Components	18
Table 6. Electrochemical History of a Single Positive Electrode From a Commercial Nickel-Cadmium Battery	19
Table 7. Electrochemical History of a Single Negative Electrode From a Commercial Nickel-Cadmium Battery	26
Table 8. Energy-Output Densities as a Function of Charging-Current Density After 30 Percent Overcharge	37

DEVELOPMENT OF LARGE-INTERNAL-SURFACE-AREA NICKEL METAL PLAQUES

by

J. McCallum, G. R. Schaer, D. G. Trevethan, and C. L. Faust

INTRODUCTION AND OBJECTIVES

As described in the First Quarterly Progress Report, the specific objective of this program is the development of porous nickel metal plaques for the rechargeable cadmium electrode to provide higher energy output per unit of weight than is presently available. To achieve this specific objective, the research has three general objectives:

- (1) Explore the possibilities for stacking electroformed screens into plaque structures with a uniform pore distribution
- (2) Control pore shapes by selective electroforming and stacking procedures
- (3) Demonstrate the physical and electrical advantages for the controlled pore shapes in nickel plaques.

During the first quarter of work, the feasibility was established of stacking electroformed screens into plaque structures with a uniform pore distribution. The first quarter of work also commenced the classification of presently used battery plaques, both physically and electrochemically. Chemical impregnation procedures were worked out. Electrochemical evaluations were started on commercial batteries and battery plaques to provide references with which to judge new electrode structures.

During this second quarter of the work, therefore, the objectives were as follows:

- (1) Using stacking techniques developed during the first quarter, make experimental electrodes in accordance with the requirements of Task B, having a range of pore sizes
- (2) Complete the characterization of commercial materials as required for reference data
- (3) Using impregnation procedures standardized during the first quarter, commence the electrochemical evaluation of newly made experimental electrodes.

Within each of these objectives for the second quarter, there are subsidiary objectives that will be apparent in the descriptions of each task of the program.

SUMMARY

Toward the objective of manufacturing experimental porous plaques with controlled pore size and shape, electroformed screens of 250, 500, 750, and 1000 mesh have been stacked and bonded into structures 5 to 21 mils thick. The pores are essentially square and are continuous through the mat. The stacking machine and the procedures and parts associated with it are being improved constantly. Each new stack appears to be better aligned than the previous one, and reasonably satisfactory alignment has been achieved.

The first electrodes have had porosities between 38 and 65 percent; more than 50 percent porosity seems desirable before impregnation. Etching to increase porosity of stacked screens after bonding seems to require slow etchants in nonaqueous solvents. The aqueous etching solutions have preferentially attacked grain boundaries, thereby disintegrating the wires.

New methods of physical impregnation appear to hold considerable promise for electrodes that have holes perpendicular to the flat faces. For example, one simple pressing of cadmium metal powder or cadmium oxide powder, with one's finger, resulted in filling the same percent of voids as would result from four conventional chemical impregnation cycles.

Electrochemical evaluation procedures have been completed so that energy outputs from single experimental negative electrodes can be evaluated in three ways:

- (1) New single electrodes can be compared with commercial single electrodes under identical conditions.
- (2) New single electrodes can be compared with commercial single electrodes under a variety of conditions, including cycling and current-density variations.
- (3) Results with new single electrodes can be related to expected improvements in sealed cells or batteries of sealed cells.

Conversion factors and standards for the above energy-output evaluations have been determined so that future work can proceed as called for in the contract.

Energy-input studies have commenced. Enough data on commercial electrodes seem to have been obtained during this report period to provide standards for evaluating results with future experimental electrodes.

Microscopic studies of negative electrodes after repeated deep cycling showed that the active cadmium metal powder shifted from large pores into small pores without a significant change in total weight. This migration of cadmium was unknown prior to this work and can account for the loss in capacity that has been reported by others. Work with experimental screen electrodes having random pore sizes showed that the electrodes with the largest pores had the least loss after five charge-discharge cycles. Electrode structures with uniform pore sizes can be expected to eliminate the loss of capacity because of the shifting of the cadmium metal powder.

FUTURE WORK

Details of future-work plans are given for each task in the pertinent sections of this report. In brief, the planned work is aimed toward the following accomplishments during the next monthly reporting period:

Task B - Porous Mat Manufacture

- (a) Complete stacking of screen-type mats with superimposed holes
- (b) Evaluate a new method of stacking screens whereby screens are stacked and spot welded one at a time
- (c) Continue the study of new chemical etchants for increasing the porosity of stacked and bonded screen mats

Task E - Impregnation Procedure

The work on physical impregnation will be postponed for 1 month, but will consist of refining methods of impregnating screen mats with cadmium metal powder.

Task F - Electrochemical Evaluation

Experimental screen mats will be electrochemically evaluated as they become available from Task E.

EXPERIMENTAL WORK BY TASKS

The First Quarterly Progress Report itemized and discussed the research on each task as listed in the contract. The sections that follow are arranged in accordance with that format. Only new data and discussions are given in this quarterly report.

Task A - Raw Material Classification

This task was completed and described in the First Quarterly Progress Report, pages 4-13. Classification of experimental plaques will be continued as part of Task D.

Task B - Porous Mat Manufacture

Objectives

The objectives of this task are to

- (1) Determine an optimum electrode thickness as a function of pore size
- (2) Develop laboratory methods for electroforming and building porous plaques according to advance specifications
- (3) Provide a variety of predetermined pore shapes for experimental study.

Item 1 - Thickness Range

The thickness and screen mesh selected for construction are

<u>Screen Mesh, lines/inch</u>	<u>Thickness, mils</u>
250	5, 10, 21, 35
500	5, 10, 21, 35
750	5, 10
1000	5, 10

During this report period, the following thicknesses were prepared:

<u>Screen Mesh, lines/inch</u>	<u>Thickness, mils</u>	<u>Pore Size, mils</u>	<u>Weight, mg</u>	<u>Volume, ml x 10⁻³</u>	<u>Porosity, percent</u>
250	3.3	3.2	25.8	8.4	65
500	7.4	1.2	103.6	18.8	38
250	6.8	2.6	67.1	14.0	46

The remaining thicknesses are being prepared.

Item 2 - Techniques for Making Mats

Stacking Screens. Screens have been stacked with superimposed holes using the special stacking machines described on page 18 of the First Quarterly Progress Report.

Improvement in positioning accuracy of stacked screens was obtained by making almost zero clearance between the punch and die. This has been accomplished by making a die slightly undersize, then broaching the hole in the die to size with the punch to be used in punching out screen sections. Dies were reconditioned and reused by plating with nickel to make the hole through the die undersize, then broaching with a punch. Clearances up to 0.1 mil between the punch and die were obtained by electropolishing

the nickel plate to remove the desired thickness of metal. A thin chromium plate of 0.01 mil was applied to the dies to improve shearing action and resist galling of the nickel screen on the nickel-plated die.

The best alignment of holes in stacked screens has been obtained with 250- or 500-mesh screens, each about 0.5 to 1.0 mil thick.

Figures 1 through 10 are photomicrographs of three sets of stacked electroformed screens which show how the holes were superimposed. Figures 1, 2, 5, and 8 show the top surface of screens before the heat-bonding operation. Figures 3, 6, and 9 show this same top surface after the heat-bonding step. Figures 4, 7, and 10 show the bottom surface of the three stacks of screens after bonding.

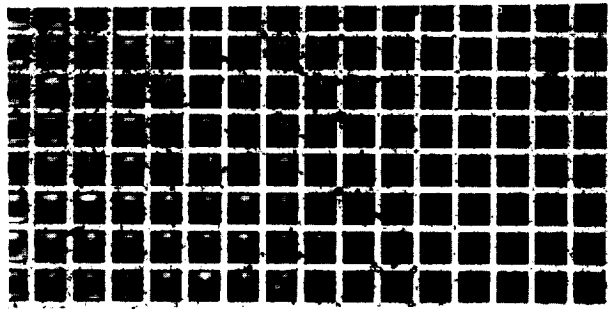
Figures 1 and 2 are of the same specimens photographed under different conditions to show alignment. Figure 1 was taken with the microscope focused on the top layer. Layers underneath the top screen do not show. Figure 2 was taken with the microscope focused on a layer beneath the top layer. Note the alignment is good but not perfect. Figures 1 and 5 are both of 250-mesh screens. The screen in Figure 1 had about 60 percent openings, whereas the screen in Figure 5 had about 25 percent openings.

After the heat-bonding step, all of the nickel screen structures show crystal growth in the metal. This is normal for annealed-nickel electroplated metal. However the increase in crystal size influenced the etching results, as described in the section Control of Porosity.

A new technique for stacking and bonding screens will be checked. Screens will be placed one at a time on a stack and positioned by hand using a microscope to check alignment. Each layer will be spot welded in several spots to hold the screens in place. Bonding of the stacked layers will be done by heating in a hydrogen atmosphere. The advantage of this method is that larger sections can be fabricated than by the punch and die method.

Electroforming Screens. Nickel screens of 175 or 250 mesh have been electroformed on flat reusable mandrels. The mandrels, described in the First Quarterly Progress Report, page 17, were prepared in the following way: Copper panels were etched with a hole pattern corresponding to holes in screens, and the holes were filled with acid-resisting glass (vitreous enamel). Polishing of the glass to expose the raised copper cell structure followed by buffing the copper and chromium plating gave a surface suitable for electroforming nickel screens. The glass is considered to be preferable to plastic materials because it (1) adheres better, (2) resists chemical attack, and (3) is stronger. However, the glass is harder to polish to expose the copper cell structure. Ten screens were electroformed on a 1 by 2-inch mandrel with no evidence of chemical attack on the glass. Composition of the glass was:

Component	Formula	Weight, grams	Component	Formula	Weight, grams
Lithium carbonate	Li_2CO_3	92	Copper oxide	CuO	136
Sodium carbonate	Na_2CO_3	352	Lead silicate	PbSiO_3	1932
Sodium nitrate	NaNO_3	180	Sodium silicofluoride	Na_2SiF_6	60
Silica	SiO_2	1024	Boric acid	H_3BO_3	64
Titanium oxide	TiO_2	120			

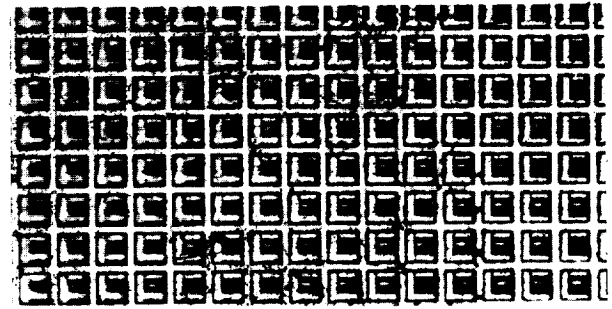


100X

19793

FIGURE 1. TOP SURFACE OF SUPERIMPOSED 250-MESH
SCREENS BEFORE BONDING

Focused on top screen.

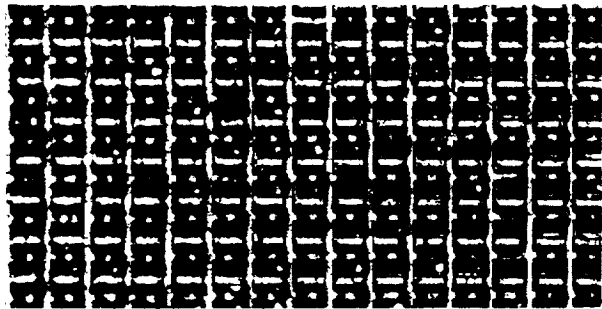


100X

19794

FIGURE 2. TOP SURFACE OF SUPERIMPOSED 250-MESH
SCREENS BEFORE BONDING

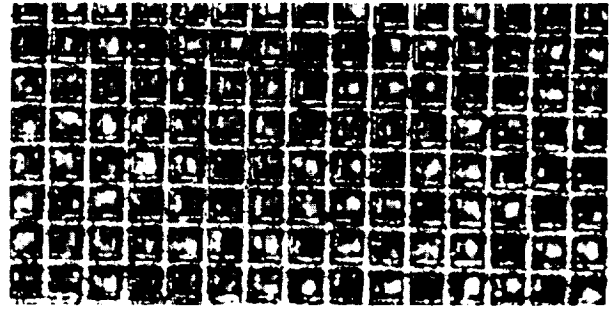
Focused on underneath layer.



100X

19795

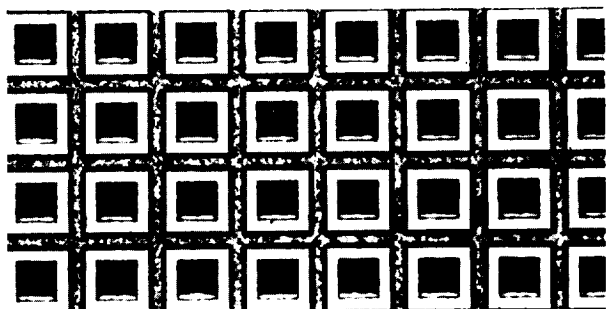
FIGURE 3. TOP SURFACE OF SUPERIMPOSED 250-MESH
SCREENS AFTER BONDING



100X

19796

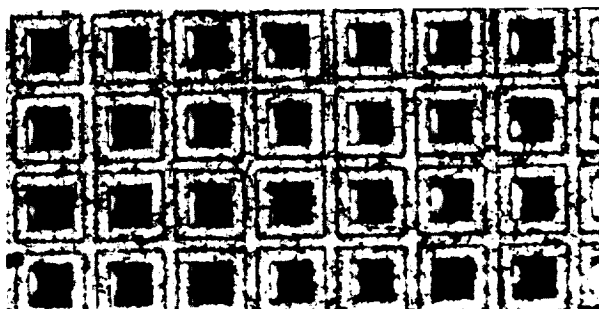
FIGURE 4. BOTTOM SURFACE OF SUPERIMPOSED
250-MESH SCREENS AFTER BONDING



100X

19797

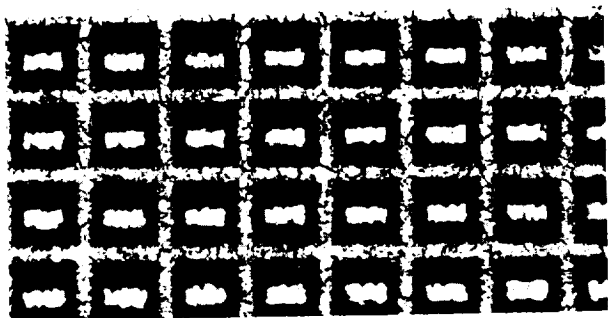
FIGURE 5. TOP SURFACE OF SUPERIMPOSED 250-MESH SCREENS BEFORE BONDING



100X

19798

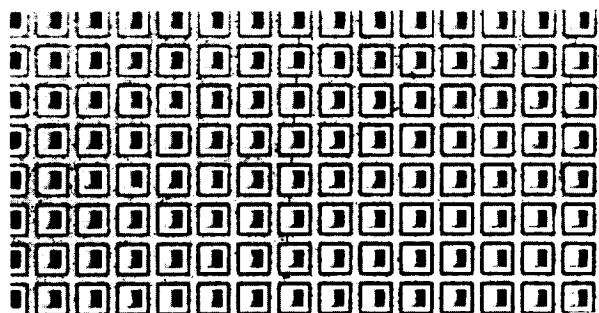
FIGURE 6. TOP SURFACE OF SUPERIMPOSED 250-MESH SCREENS AFTER BONDING



100X

19799

FIGURE 7. BOTTOM SURFACE OF SUPERIMPOSED 250-MESH SCREENS AFTER BONDING



100X

19800

FIGURE 8. TOP SURFACE OF SUPERIMPOSED 500-MESH SCREENS BEFORE BONDING

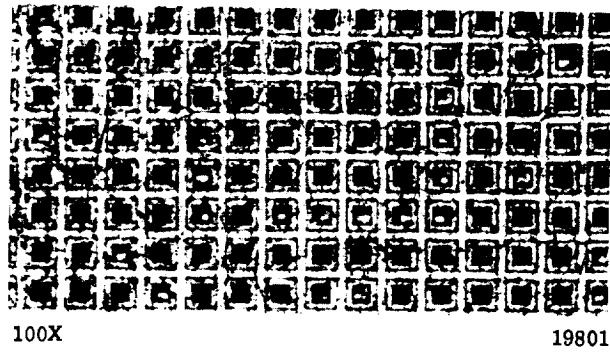


FIGURE 9. TOP SURFACE OF SUPERIMPOSED 500-MESH
SCREENS AFTER BONDING

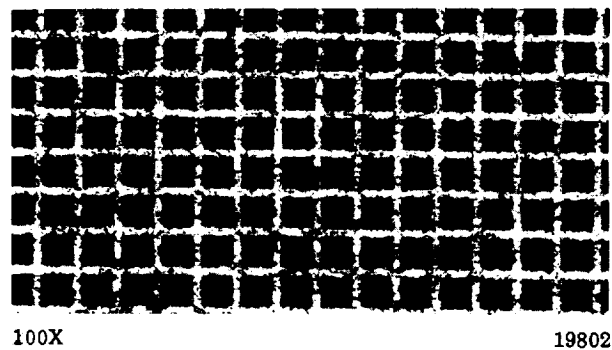


FIGURE 10. BOTTOM SURFACE OF SUPERIMPOSED 500-MESH
SCREENS AFTER BONDING

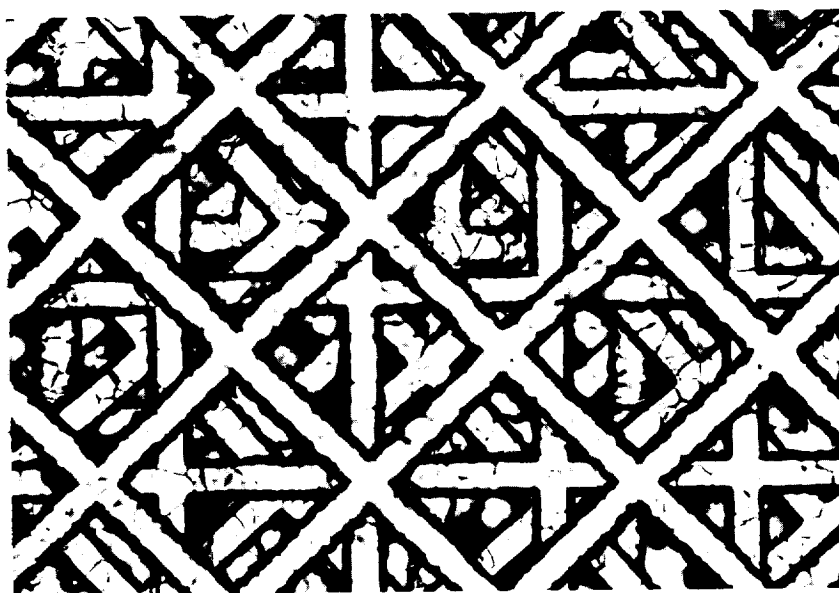
Air bubbles were removed from the glass during firing by applying a vacuum of 150 to 200 microns for about 2 minutes after the slip-coated mandrel had been heated for 6 minutes at 1450 F in a nitrogen atmosphere. Nitrogen was used to prevent oxidation of the copper. The coated mandrels were cooled in a nitrogen atmosphere.

Mandrels with 2 by 4-inch screen patterns have been etched and glass coated with mesh sizes of 175, 250, and 500. They will be finished and used for electroforming screens. Positioning holes will be electroformed along the edges for alignment pins. Stacking will be done with pins to make the screens register.

Item 3 - Methods for Controlling Pore Shapes

To date, two pore shapes have been made and evaluated. Straight-through pores were made with the stacking machine described earlier. Semirandom pore shapes were made by stacking screens with square holes with approximately 45-degree orientation of wire. Such stacking gives an essentially random shape to pores, but pore sizes cannot be larger than a single square hole of one screen. Pore sizes cannot be smaller than the thickness of a single screen, for screens which have a hole size larger than the thickness of the screen.

The semirandom-orientation screen structure is shown in Figure 11. Screens were stacked by turning alternate layers about 45 degrees. No attempt was made at any other preferred positioning. In Figure 11, the microscope was focused on the third layer from the top. Screens above and below were slightly out of focus.



200X

N19054

FIGURE 11. SURFACE VIEW OF STACKED AND BONDED 250-MESH SCREENS - SEMIRANDOM ORIENTATION

Control of Porosity. Commercial electroformed screens used in this work have 25 to 60 percent openings. Stacks made with these screens have, therefore, 25 to

60 percent porosity. Electrochemical evaluations are more meaningful if all experimental electrodes have the same percent porosity. The relationship of hole size, porosity, and mesh size is shown in Table 1. To experimentally compare the effect of pore size and pore length, high porosity is not needed.

TABLE 1. RELATIONSHIP OF HOLE SIZE AND POROSITY OF SCREENS

Mesh, lines/inch	Size Center to Center, mil	Hole Width, h, mils	Wire Width, w, mils	Ratio, w/h	Percent Openings ^(a)
1000	1.0	0.95	0.05	0.05	90
1000	1.0	0.90	0.10	0.11	81
1000	1.0	0.85	0.15	0.18	72
1000	1.0	0.80	0.20	0.25	64
1000	1.0	0.70	0.30	0.43	49
750	1.33	1.27	0.07	0.05	90
750	1.33	1.20	0.13	0.11	81
750	1.33	1.14	0.20	0.18	72
750	1.33	0.07	0.27	0.25	64
750	1.33	1.00	0.33	0.43	49
500	2.0	1.9	0.1	0.05	90
500	2.0	1.8	0.2	0.11	81
500	2.0	1.7	0.3	0.18	72
500	2.0	1.6	0.4	0.25	64
500	2.0	1.4	0.6	0.43	49
250	4.0	3.8	0.2	0.05	90
250	4.0	3.6	0.4	0.11	81
250	4.0	3.4	0.6	0.18	72
250	4.0	3.2	0.8	0.25	64
250	4.0	2.8	1.2	0.43	49

(a) Assuming wires have rectangular cross sections.

A program is under way to chemically etch stacked nickel screens to increase porosity to about 60 percent. Etching solutions have been devised that remove metal at different rates, depending on agitation. Such a solution when flowed through stacked screens has the potential of removing metal faster from the projecting sides of the wires than from the top and bottom, where the wires are joined. Table 2 shows etching rates of ferric chloride solutions on 1/4-inch-nickel rods with and without agitation. The solution of ferric chloride and hydrochloric acid which had the highest ratio (10 to 1) was checked on both a single screen and on stacked and bonded screen. The screen was placed between two filter papers and the solution flowed through the screen and filter papers with a vacuum and filter flask. The filter paper was considered necessary to restrict the flow through the screen. Without the restriction, flow rates through all the holes would be about the same. With the restriction, volume of solution flowing through each hole should be nearly the same. Therefore, small holes (or restrictions in any hole) due to slight misalignment of layers would have a higher flow rate and be etched faster. Thus, holes should be made more uniform in size and width.

TABLE 2. NICKEL ETCHING RATES IN FERRIC CHLORIDE SOLUTIONS

Solution	Bath Composition					Weight Loss in 5 Minutes		
	FeCl ₃ , g/l	HCl (37%), cc/l	Temperature,		Additives	Weight Loss, mg/in. ²		Ratio of Weight Loss, agitation/no agitation
			F	pH		Agitation	No Agitation	
1	570	0	74	<0	--	41	17	2.4
2	570	0	74	<0	Dimethylglyoxime	40	16	2.5
3	570	0	74	<0	Thioacetamide	53	20	2.6
4	570	0	74	<0	Thiourea	24	14	1.7
5	140	0	72	1.6	--	58	16	3.6
6	70	0	72	1.7	--	38	7	5.4
7	70	0	75	3 to 4	NaOH	35	8	4.4
8	3	10	80	--	--	10	1	10.0

With a single thickness of an electroformed screen in the as-plated condition, flowing etching solution (Solution 8, Table 2) through the screen for about 5 minutes reduced the wire width by 1 mil and the thickness by 0.3 mil. This is a ratio of about 3.3 to 1 for the high to low agitation areas on the wires.

Stacked and bonded screen plaque with semirandom orientation was etched for 1 minute under the same conditions used for the single layer screen. One minute of treatment time was selected because the expected etching would reduce the wire width from 0.8 to 0.6 mil. However, the screen disintegrated into powder. Examination of the residue showed short lengths of wire. Judging by microscopic examination, the nickel screens recrystallized during bonding so that each wire was a series or chain of crystals, many of which were the full width of the wire. The etching solutions apparently attack the crystal boundaries faster than the crystals and cut through the wires, causing disintegration of the structure. No aqueous solution is known that will attack the crystal boundaries at the same or lower rate as it will the crystals of nickel.

Alkaline solutions of ferricyanide with sodium cyanide and sodium cyanide and hydrogen peroxide did not seem to attack nickel at any significant rate. More exotic solution such as bromine in alcohol could etch nickel uniformly. This mixture was reported for stripping oxide coating from stainless steel and chromium and will be tested in future work.

Future Work

- (a) Evaluation of new etchants for increasing porosity of bonded screen structures will be continued.
- (b) Evaluation of a method for superimposing screens by aligning one layer of a screen and spot welding it into place before aligning the next layer.
- (c) Continue stacking of 1 x 1-cm superimposed screen for electrochemical evaluation using the stacking machine.

Location of Data

All experimental data on Task B are contained in Battelle Laboratory Record Books, Nos. 21516, pages 24 to 50; 21595, pages 18-23; and 21867, pages 1-12.

Task C - Sintered-Plaque Processing

The details of conditions selected for sintering stacked screens are given in the First Quarterly Progress Report, pages 19-21. These conditions will be modified only as needed to increase the quality of experimental electrodes.

Task D - Plaque Classification

Commercial sintered powder nickel plaques were classified during the First Quarterly Progress Report period. Eight physical properties were determined with which new electrodes can be compared. The results are summarized as follows for 21-mil-thick commercial plaques:

- (1) Electrical restivity, edge to edge - 159 μ ohm-cm
 surface to surface - 173 μ ohm-cm

- (2) Pore-size distribution

<u>Pore Diameter,</u> <u>mils</u>	
Maximum	14
Minimum	0.13
Average	0.63

Range to include 66% of volume 0.41 to 1.4

- (3) Pore shapes, random
- (4) Internal surface area, 0.088 m²/g
- (5) Density, 1.85 g/cm³
 Porosity, 79 percent voids
- (6) Interconnecting pores, 100 percent
- (7) Tensile strength

	<u>To Cracking of</u> <u>Nickel Powder</u>	<u>To Failure of</u> <u>Supporting</u> <u>Wire Screen</u>
Tensile strength, psi	1700	2600
Yield strength (0.2% offset)	1000	1000
Elongation (1-inch gage), percent	3	14

BATTELLE MEMORIAL INSTITUTE

- (8) Flexibility, cracking of powder during first 90-degree bend over a 0.5-cm radius using the test described in ASTM Standards A 344-60T.

Newly made experimental electrodes will be compared with the above values after promising structures have been selected on the basis of results from Task F.

Task E - Impregnation Procedure

Objectives

The objective is to evaluate at least two different methods of impregnating porous nickel structures with cadmium hydroxide. The methods noted in the contract are chemical impregnation, which has been completed, and physical packing.

Physical Packing Methods

The plaque structure with straight-through holes made with stacked screens is more amenable to physical packing methods than is the structure of sintered nickel powder with random pores. Cadmium powders, cadmium oxide, and cadmium hydroxide were checked for bulk densities to determine whether enough of these materials could be packed in the pores to give sufficient capacity. Screen plaques were physically impregnated with cadmium oxide or cadmium metal powder but not cadmium hydroxide. The semirandom pore shape was used because plaques with superimposed holes were not available for this part of the experimental program. However, if the random pore shape can be impregnated, the straight-through pores should be at least as easy to impregnate.

Cadmium Metal Powder. Cadmium metal powder was produced by electrolyzing a slurry of cadmium hydroxide in 30 percent potassium hydroxide. The product was essentially the same cadmium metal powder or sponge produced in negative electrodes during charging. The powder was placed on a plaque of semirandom pore shapes and rubbed in with a finger to force the powder in the pores. On a basis of $\text{Cd}(\text{OH})_2$, the plaque had 45 percent of the pore volume filled. Four cycles of the chemical method fill about 40 percent of the voids.

Cadmium Oxide. Reagent-grade cadmium oxide powder was slurried in water and filtered, and a bulk-density measurement was made of the filter cake. On a $\text{Cd}(\text{OH})_2$ basis, the cake had a 48 percent density. Thus, if 83 percent of the pore volume of a plaque could be filled with this product, the impregnated plaque would have the capacity equivalent to that obtained with four cycles of the chemical impregnation method.

One check was made with a semirandom pore shape-stacked screen electrode with CdO forced into the pores as a slurry. On a $\text{Cd}(\text{OH})_2$ basis, 37 percent of the pore volume was filled. Alternate charge and discharge of this electrode showed 53 percent of the cadmium material was electrically available. These results are encouraging for a first trial.

Cadmium Hydroxide. A freshly prepared cadmium hydroxide filter cake had the equivalent of 9 and 19 percent theoretical density for as-filtered and for filtered and compressed conditions, respectively. Physically filling the pores of a plaque with cadmium hydroxide is considered impractical because it is unlikely that enough active material could ever be packed into the pores to give capacity equal to that obtained with the chemical impregnation.

Future Work

Additional experiments are planned for impregnating screen plaques with cadmium oxide, cadmium metal powder, or mixtures of these two. Carbon will be considered as an additive to both the oxide and the metal powder material to provide a lubricant, to prevent welding and agglomeration of particles during impregnation, and to improve conductivity of the electrode.

Location of Data

All experimental data on Task E are contained in Battelle Laboratory Record Book No. 21981, pages 1-19.

Task F - Electrochemical Evaluation

Objectives

The objectives of this task during the report period are to

- (1) Determine standards for comparing experimental screen electrodes with commercial electrodes
- (2) Provide conversion factors that will yield predicted energy densities for commercial batteries utilizing experimental screen electrodes
- (3) Commence electrochemical evaluation of newly manufactured experimental electrodes to optimize energy output as a function of electrode geometry.

Item 1 - Energy Output

For all studies on energy output, an attempt was made to use the same charging, or energy input, routine. This charging routine was to adjust charging current to a value that would yield 100 percent of the expected ampere-hour output in a 24-hour charging period.

All experiments were performed at ambient room temperatures of 70 to 80 F.

Relationship of Cell Components to Commercial Cells

The objective of this part of the work is to provide physical and electrochemical data that can be used for evaluating future work. The first step is to provide weight and size data on the various components of a sealed cell. The second step is to provide electrochemical data for a complete cell, both sealed and with flooded electrodes. The third step is to combine the data into conversion factors that will permit new data to be used for predicting the performance of sealed cells or complete batteries.

Weight and Size Breakdown. A single cell was dismantled and dimensions were obtained on the various parts. Each cell had the overall dimensions described in Table 7 of the First Quarterly Progress Report. Each cell had three negative cadmium electrodes and two positive nickel electrodes. Cells were completely discharged to zero terminal voltage before dismantling. Weight and dimensions are given in Table 3.

TABLE 3. PHYSICAL DIMENSIONS FOR SEPARATE COMPONENTS OF A COMMERCIAL NICKEL-CADMIUM CELL

Cell Parts	Weight, g	% of Total	Volume, in. ³	% of Total
(1) Case material	11.67	23.6	0.538	32.61
(2) Sealant	1.12	2.28	0.018	1.09
(3) Terminals	5.84	11.9	0.050	3.03
(4) Separator	0.66	1.34	0.065	3.94
(5) Negative plates	14.5	29.5	0.237	14.4
(6) Positive plates	9.96	20.3	0.181	10.9
(7) Cadmium hydroxide Cd(OH) ₂	6.75	13.7	0.085	5.15
(8) Nickel hydroxide Ni(OH) ₂	4.11	8.35	0.064	3.88
(9) Nickel plaques, negative, including grids	7.75	15.7	0.054	3.28
(a) Iron grids	2.03	4.13	0.015	0.91
(10) Nickel plaques, positive, including grids	5.85	11.9	0.041	2.48
(a) Iron grids	1.35	2.75	0.010	0.61
(11) Electrolyte	5.30	10.8	0.250	15.2
(12) Free space (gas space)	--	--	0.281	17.0
Totals, measured	49.3		1.65	

Each negative electrode in the cell was 4.47 cm tall, 3.76 cm wide, and 0.08 cm thick, exclusive of electrical connection tabs. The positive electrodes had the same area but were 0.09 cm thick.

In Table 3, Items 1, 2, 3, 4, 5, and 6 were weighed wet as dismantled from the cells. They were then washed and dried to constant weights to give the data showing in the Table. Any losses of weight brought about by washing were added to electrolyte weights, assuming 30 weight percent potassium hydroxide. The sealant, Item 2, includes rubber grommets and a safety valve.

Item 7 was determined by chemical analysis, as described later. Item 8 was estimated from electrochemical data given in Table 6.

Items 9 and 10 were obtained by the difference between weights of total plaques (Items 5 and 6) and weights of active material (Items 7 and 8). That is, $(9) = (5) - (7)$ and $(10) = (6) - (8)$.

Item 11 is the sum of collected free electrolyte plus weight changes in other components.

The free electrolyte accounted for only 0.30 gram, as most of the electrolyte was contained within the plates and the separator. A breakdown of electrolyte weights in the dismantled cell is as follows:

Free electrolyte	0.30
From Separator	2.31
From 3 negative plates	1.62
From 2 positive plates	<u>1.07</u>
Total electrolyte weight	5.30 grams

Item 12 is the difference between internal case volume and the volume of the electrode assembly, as measured by the volume of liquid required to completely fill a cell.

Duplicate weight measurements on two cells showed the data in Table 3 are accurate to ± 0.15 gram or ± 5 percent, whichever is the smaller error. Volume measurements are also accurate to ± 5 percent.

The most significant conclusion, for the research objective of reducing cell weights and sizes, is that the negative plates (Item 5) are the largest single component of weight. That is, Item 5 contains the greatest percentage of total weight and would remain so even in large batteries. Therefore, any decrease in the weight of plaques (Item 9) and increase in the weight of active material (Item 7) will significantly decrease the weight of a battery.

Reproducibility. The ampere-hour capacity from a sealed cell can be measured reproducibly. As noted in the First Quarterly Progress Report, page 30, a properly charged cell or battery will give reproducible discharge capacity to ± 3 percent. Cycles 1 and 2, Table 4, show the first reproducible results.

TABLE 4. EFFECT OF FLOODING IN A COMMERCIAL NICKEL-CADMIUM CELL

<u>Input</u>	<u>Ampere-Hours</u>	
Per cell, sealed, Cycle 1	1.02	
Per cell, sealed, Cycle 2	1.02	
Per cell, flooded, Cycle 3	1.02	
Per cell, flooded, Cycle 4	1.20	
Per cell, flooded, Cycle 5	1.20	

<u>Maximum Output</u>	<u>Discharge Rate, hours</u>	<u>Ampere-Hours</u>
Per cell, sealed, Cycle 1	1.5	0.939
Per cell, sealed, Cycle 2	1.5	0.917
Per cell, flooded, Cycle 3	1.5	0.944
Per cell, flooded, Cycle 4	1.5	0.915
Per cell, flooded, Cycle 5	1.5	0.963

The first five cycles with complete cells combined with Cycle 6 in the positive electrode, Table 6, show that the output capacity of the positive plate is unchanged by deep cycling. That is, the ampere-hour capacity of the positive plate remains reproducible after six full charge-and-discharge cycles at constant rates. However, Cycles 9P, 10P, and 11P show that the measured capacity is a function of rate of discharge. Therefore, the ampere-hour capacity from a sealed cell must be measured at constant rates to obtain reproducible results.

Effect of Flooding. The ampere-hour capacity of a sealed cell will remain the same even if the cell is dismantled and the electrodes flooded with electrolyte.

Cycles 3, 4, and 5, of Table 4, show that the same outputs are obtained with flooded electrodes as were obtained with the sealed cell. Details of these experiments are given in connection with Table 8 of the First Quarterly Progress Report, pages 30-31. The practical significance of this result is that new experimental electrodes can be evaluated in beakers of electrolyte, thereby greatly simplifying the laboratory work.

Energy-Conversion Factors. The simplest procedure for estimating cell or battery performances from the performance of separate parts is to use units of lb/whr (pounds/watt hour) and in.³/whr (cubic inch/watt hour) for each part. Such units are additive whereas the more common reciprocal units of whr/lb and whr/in.³ are not additive.

By definition,

$$(\text{lb/whr})_{\text{Total}} = \text{Sum } (\text{lb/whr})_{\text{Each Part}}$$

$$(\text{in.}^3/\text{whr})_{\text{Total}} = \text{Sum } (\text{in.}^3/\text{whr})_{\text{Each Part}}$$

Using 1.15 watt-hours measured from Figure 16 of the First Quarterly Progress Report and the weights and volumes of each component in Table 3 of this report, the values shown in Table 5 were calculated for a cell. Using the watt-hours from five cells and the weight and sizes of battery-case materials*, a total battery value was calculated.

TABLE 5. APPROXIMATE WEIGHT AND VOLUME FACTORS FOR ESTIMATING PERFORMANCES FROM INDIVIDUAL COMPONENTS

Cell Part	Lb/Whr	In. ³ /Whr
(1) Case material	0.0223	0.468
(2) Sealant	0.0021	0.016
(3) Terminals	0.0112	0.043
(4) Separator	0.0013	0.056
(5) Negative plates	0.0277	0.206
(6) Positive plates	0.0191	0.157
(11) Electrolyte	0.0102	0.208
(12) Free space	--	0.245
Total Cell	0.0939	1.399
(13) Battery case	0.0597	0.386
(14) Battery free space	--	0.196
Total Battery	0.1536	1.981

This method of presentation has the advantage that it shows quickly the relative importance of each item on the overall weight and volume. Suppose, for example, the lb/whr and in. ³/whr of the negative electrode, Item 5 in Table 5 were each decreased 50 percent. The following changes would be predicted:

	Present Value, lb/whr	Predicted New Value, lb/whr	Percent Decrease	Present Value, in. ³ /whr	Predicted New Value, in. ³ /whr	Percent Decrease
Negative plates	0.0277	0.0138	50	0.206	0.103	50
Total cell	0.0939	0.0800	17.4	1.399	1.296	7.4
Total battery	0.1536	0.1397	9.5	1.981	1.878	5.2

This method of calculation has another advantage in that manufacturers, or other workers in the field, can use new data with their own data expressed in the same units. Thus, a different case arrangement might change Items 1, 2, 12, and 13, in Table 5 without changing the other factors.

*First Quarterly Progress Report, Table 7, p 29.

The method has a disadvantage because it implies that each component can change independently. In actuality, an improvement in any one component can change the observed values for other components. Improved electrodes might be packed in the same containers, for example, thereby changing values for case materials, sealant, terminals, separators, electrolyte, and free space. This is a complication that need not be dealt with on the present project to show improvements in negative electrodes.

Commercial Single Positive Electrodes

Following the above results with sealed and flooded cells, single-electrode measurements were commenced. Details of the experimental procedures with single electrodes are given in a later section, Evaluation Method.

The majority of future work will be concerned with measurements on single negative electrodes. But in order to relate future results to their effect on total cell or battery performances, data must be obtained on single positive electrodes under identical conditions.

Effect of Rate of Discharge. Cycles 9P, 10P, and 11P (Table 6) show the rate dependence of the positive electrode. Less capacity is obtained at higher discharge rates, which is to be expected, since the electrode efficiency is a function of current density. Thus, the maximum capacity should be expected from Cycle 10P, which had the lowest rate of discharge. However, the values obtained from 9P and 10P are similar within experimental error, and the highest capacity value will be used as theoretical in this report. Ritterman and Seiger report that a 50-hour rate is required to achieve theoretical capacity at a positive electrode.*

TABLE 6. ELECTROCHEMICAL HISTORY OF A SINGLE POSITIVE ELECTRODE FROM A COMMERCIAL NICKEL-CADMIUM BATTERY

<u>Input</u>	<u>Ampere-Hours</u>	
Per positive, flooded, Cycle 6P	0.60	
Per positive, flooded, Cycle 7P	0.60	
Per positive, flooded, Cycle 8P	0.60	
Per positive, flooded, Cycle 9P	0.80	
Per positive, flooded, Cycle 10P	1.60	
Per positive, flooded, Cycle 11P	0.84	
<u>Maximum Output</u>	<u>Discharge Rate, hours</u>	<u>Ampere-Hours</u>
Per positive, flooded, Cycle 6P	1.5	0.477
Per positive, flooded, Cycle 7P	5	0.485
Per positive, flooded, Cycle 8P	11.5	0.479
Per positive, flooded, Cycle 9P	24	0.594
Per positive, flooded, Cycle 10P	45	0.581
Per positive, flooded, Cycle 11P	1.5	0.528

*Ritterman, P., and Seiger, H. N., Gulton Industries, Inc., "Investigation of Battery Active Nickel Oxides", Quarterly Progress Report (September 11, 1964).

A second result to be deduced from Table 6 is the current densities that correspond to the more conventional units of hours for discharge rate. Current density is the variable that determines the majority of an electrode polarization. A constant current density should be used when electrode thickness is varied, to provide realistic comparisons.

The electrodes in Table 6 and in Figures 12 and 13 were $4.47 \times 3.76 \times 0.090$ cm. The total area was, therefore, 33.6 cm^2 for both sides. The current for a 1.5-hour rate of discharge was 320 milliamperes, giving 9.54 ma/cm^2 as the current density equivalent to the 1.5-hour rate of discharge.

However, the commercial electrodes had a small perimeter of supporting grid on which sintered powder was missing. And since future experimental electrodes will be 1×1 -cm plaques without an inert perimeter, this small area difference was accounted for as follows: The area of sintered plaque was 4.27×3.47 cm, or 29.6 cm^2 on both sides. A 320-milliamperes discharge would then correspond to 10.8 ma/cm^2 for the 1.5-hour rate.

Figure 14 summarizes the average half-cell potentials for positive electrodes, where the 10.8 ma/cm^2 point corresponds to the 1.5-hour rate of discharge. Other hourly rates of discharge are inversely proportional to current density. For example, 16.2 ma/cm^2 corresponds to a 1.0-hour rate of discharge and 5.4 ma/cm^2 corresponds to a 3.0-hour rate.

The voltages in Figure 14 are the midpoint voltages between beginning and the end of discharge at each current density from the voltage-time curves given in Figures 12 and 13. Subsequently, the voltage values in Figure 14 will be added to observed values for single negative electrodes to provide a cell voltage for calculation of watts.

Oxygen Effect. Note that the discharge curves for the single positive electrode, 6P through 10P as shown in Figures 12 and 13, are composed of a primary and secondary discharge reaction. S. Uno Falk reports that the secondary discharge stage of the positive electrode is probably caused by oxygen adsorbed by Ni(OH)_2 .^{*} Thus, to obtain true capacity from the positive electrode, a voltage cut-off of zero volt with respect to the saturated calomel reference electrode has been used to eliminate the oxygen effect.

Commercial Single Negative Electrodes

New experimental electrode structures will be evaluated as single negative electrodes. A first step, therefore, is to provide analogous data for commercial single negative electrodes as a reference for evaluating new data. This section of the report describes (1) methods and results with single negative electrodes and (2) how laboratory data might be used to predict performances of sealed cells and batteries.

Chemical Analysis. As a means for calculating theoretical values and efficiency of utilization of active materials, commercial negative electrodes were chemically analyzed.

^{*}Falk, S. Uno, J. Electrochem. Soc., 107, 662-663 (1960).

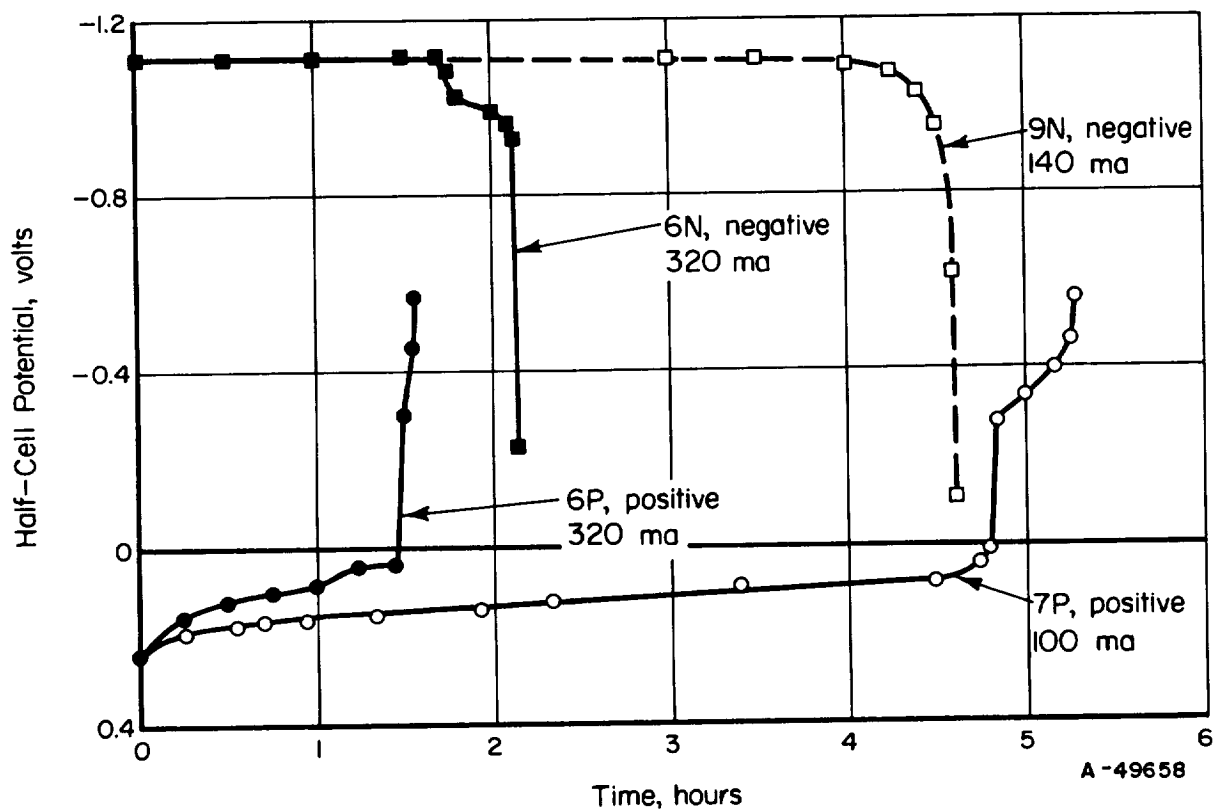


FIGURE 12. HALF-CELL DISCHARGE DATA FROM COMMERCIAL NICKEL-CADMIUM ELECTRODES

Potentials are in reference to the saturated calomel electrode.

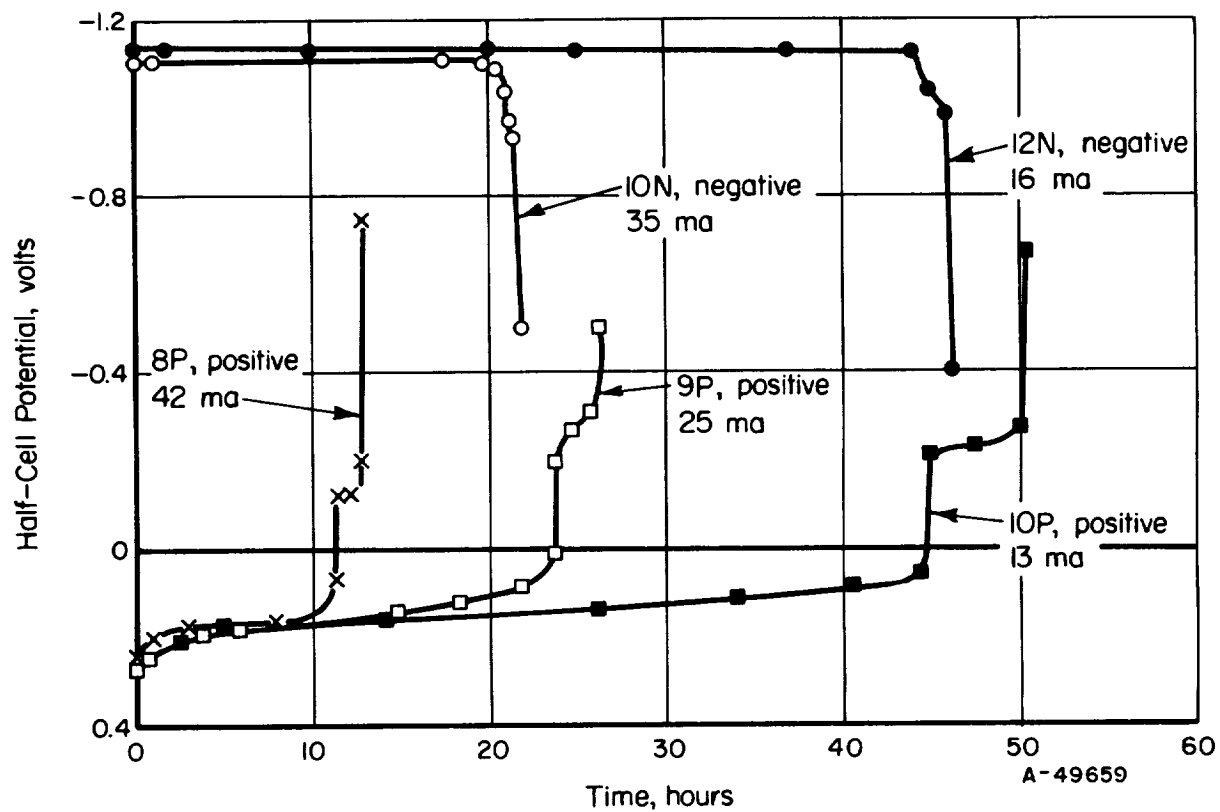


FIGURE 13. HALF-CELL DISCHARGE DATA FROM COMMERCIAL NICKEL-CADMIUM ELECTRODES

Potentials are in reference to the saturated calomel electrode.

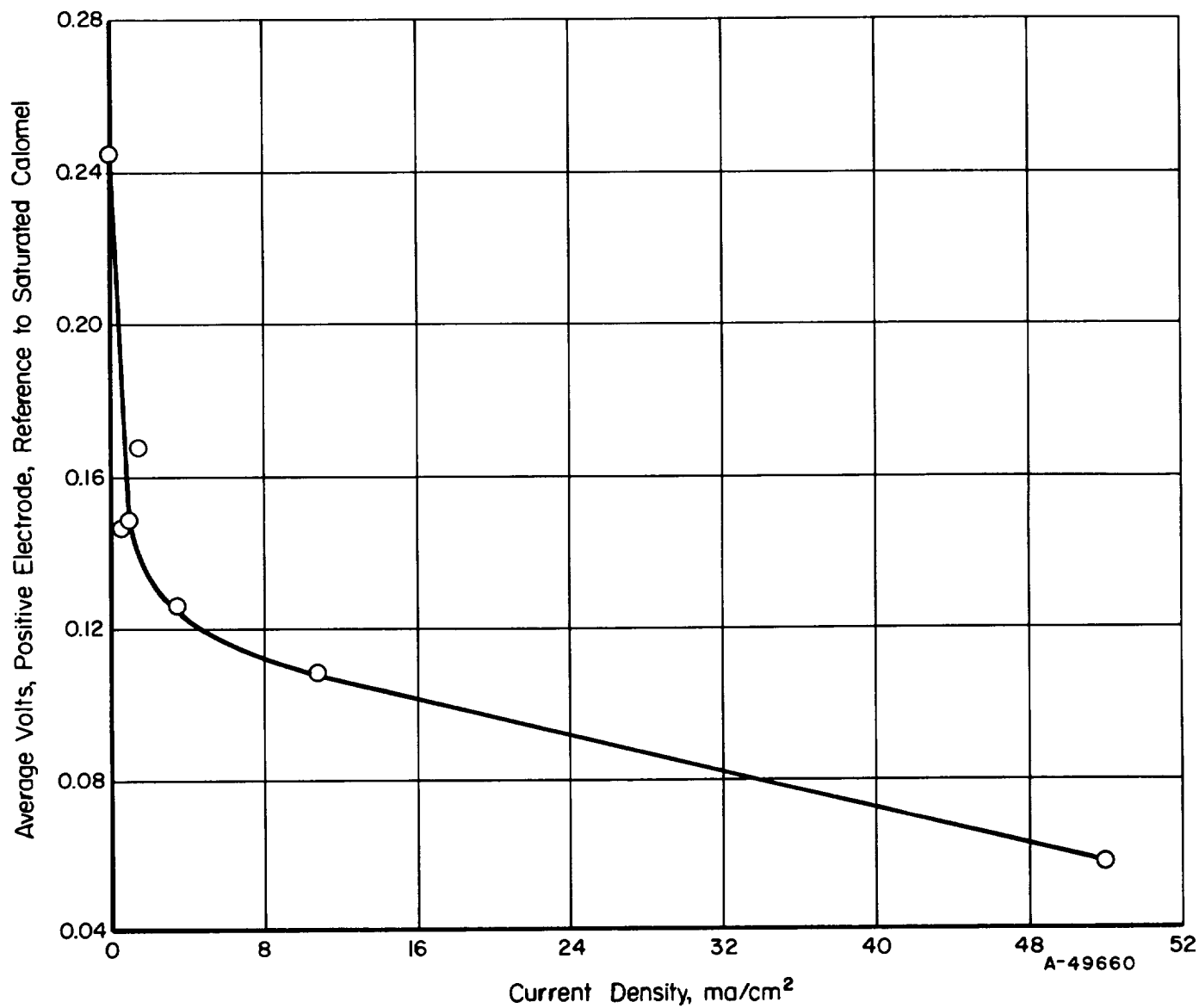


FIGURE 14. AVERAGE VOLTAGE OF POSITIVE HALF-CELL VS CURRENT DENSITY

A negative plate from the cell described in Table 3 was subjected to chemical analysis to determine its percentage composition and ampere-hour capacity. One negative plate was weighed wet with the tab removed. The recorded weight was 5.093 grams. The entire sample was dissolved in nitric acid. It was then fumed in sulfuric acid in order to permit plating of nickel. Nickel was plated and weighed as a metal. Cadmium was separated as the sulfide, then converted to the sulfate and weighed. Iron was separated by an ammonium hydroxide precipitation and determined volumetrically. The following percentage composition was reported: nickel 34.3%, cadmium 33.9%, and iron 13.3%. The remaining 18.5% was electrolyte.

Based on the weight of 5.093 grams, the following weights of metal were reported: nickel 1.747 grams, cadmium 1.727 grams, and iron 0.677 gram. The remainder of the weight, 0.942 gram, was electrolyte and represents a larger quantity than that reported earlier, in the section Weight and Size Breakdown, because the electrode was flooded with electrolyte before chemical analysis. The flooded electrode contained 0.942 gram of electrolyte while the sealed-battery electrode had 0.54 gram of electrolyte. Therefore, about 43 percent of the void volume in the sealed-battery electrode was free volume for oxygen diffusion for recombination. Since the active material after impregnation is reported as cadmium hydroxide, the weight of cadmium, 1.727 grams, was converted by calculation to the equivalent weight of cadmium hydroxide, 2.250 grams. Thus, the weight percentage of total solids, neglecting electrolyte weight, was 37.4 nickel, 48.1 cadmium hydroxide, and 14.5 iron.

The dimensions of the analyzed plate were 4.47 x 3.76 x 0.080 cm. Therefore, area = 16.8 cm² and volume = 1.344 cm³. Since the weight of iron was 0.677 g, the volume of the supporting iron grid was 0.086 cm³. The 1.747 g of nickel, therefore, occupied 1.258 cm³, giving an apparent density of 1.39 g/cm³, and a calculated porosity of 84.1 percent voids. The overall calculated density of the plate is 1.82 g/cm³. Assuming a density of 8.90 g/cm³ for nickel and 7.86 g/cm³ for iron, the theoretical density of the mixed metals is 8.60 g/cm³, giving an overall calculated porosity of 78.0 percent voids. This calculated porosity for a plate from a battery agrees well with 79 percent voids reported in Table 4 of the First Quarterly Progress Report for a commercial unimpregnated sintered powder plaque.

The 1.727 g of reported cadmium corresponds to 2.25 g of cadmium hydroxide whose theoretical density is 4.79 g/cm³. The theoretical volume of the cadmium hydroxide is, therefore, 0.470 cm³. The volume of voids is 78.0 percent of 1.344 cm³, or 1.050 cm³. The voids were 44.7 percent filled, according to this calculation, which is slightly higher than the 39 percent of pore volume filled with four impregnation cycles, as reported in Table 6 of the First Quarterly Progress Report.

Cadmium hydroxide, as noted above, was present in the quantity of 2.25 grams. Since 0.366 ampere-hour is obtained from 1 gram of cadmium hydroxide, the theoretical capacity for the negative electrode is 0.823 ampere-hour.

A subsequent analysis on a second negative plate checked within 2 percent of the above analytical results. All the calculations are considered, therefore, to be accurate within 2 or 3 percent.

An additional sample of a commercial negative plate was analyzed spectroscopically in order to determine whether additives, which would reduce capacity losses due to cycling, were present. In addition to the cadmium, nickel, and iron previously reported there was evidence of the following:

Silicon	<0.01%
Manganese	0.05%
Magnesium	0.05%
Copper	0.02%
Calcium	<0.01%
Aluminum	<0.01%

Indium, which is reported in the section of this report on cycle effects as a possible additive which reduces capacity losses, was not detected in the above analysis. The detection limit of the method used in the spectroscopic analysis is <0.01%. Thus, the conclusion is that no additive is used in the fabrication of the commercial negative electrode under consideration.

Experimental Methods. Standard electrodes 1 x 1 x 0.08 cm were cut from battery plaques taken from commercial cells. These electrodes were charged and discharged separately against platinum counter electrodes in beakers flooded with 30 percent KOH electrolyte.

Charging and discharging were carried out at constant current densities. The constant current was maintained by using a large voltage dropping resistor in series with the cell across an 18-volt rectifier. With this arrangement, voltage changes in the cell are negligible compared to the voltage across the dropping resistor, thereby assuring constant current.

Half-cell potentials were determined by means of a saturated calomel reference electrode. A Luggin capillary attached to the reference electrode was used to minimize the voltage drop due to the ohmic resistance of the electrolyte. Voltage measurements are believed to be accurate within ± 10 mv. The voltage-time curves were recorded using a Sargent Recorder Model MR. The experimental screen electrodes were 1 x 1 cm. Electrode thickness, which is a contract variable, is specified with the experimental data. Experimental screen electrodes are being tested in the same way.

The ampere-hour capacity was determined using a voltage cutoff of -1.0 volt for the negative electrode and zero volt for the positive electrode, both with respect to the saturated calomel reference electrode. The watt-hour capacity equals the product of the ampere-hour capacity and the average voltages. The electrode weight is defined as the dry weight after washing in the completely discharged condition. This weight corresponds also to the weight of an electrode after the completion of its formation cycling.

Effect of Rate of Discharge. Cycles 10N, 11N, 12N, and 13N, Table 7, show the rate dependence of the negative electrode on ampere-hours output. Less capacity is obtained at higher discharge rates. The maximum capacity should be expected from Cycle 12N, the 45-hour rate. However, possibly due to experimental error, maximum capacity was obtained from Cycle 10N, the 21-hour rate.

No data seem to be reported in the literature on how low a rate is required to achieve theoretical capacity of a negative electrode. However, chemical analysis of a negative electrode showed enough cadmium to provide 0.823 ampere-hour. Therefore, this value will be used as the theoretical capacity for a single negative electrode in this report. The maximum output of 0.744 ampere-hour, Cycle 10N, is 90.3 percent of the

theoretical capacity. The minimum output of 0.568 ampere-hour output is only 69.0 per cent of the theoretical capacity. There is, therefore, considerable room for improving the efficiency of utilization of active material in negative electrodes.

TABLE 7. ELECTROCHEMICAL HISTORY OF A SINGLE NEGATIVE ELECTRODE FROM A COMMERCIAL NICKEL-CADMIUM BATTERY

Input		Ampere-Hours
Per negative, flooded, Cycle 6N		0.75 ^(a)
Per negative, flooded, Cycle 7N		0.75 ^(a)
Per negative, flooded, Cycle 8N		0.75 ^(a)
Per negative, flooded, Cycle 9N		0.84
Per negative, flooded, Cycle 10N		0.84
Per negative, flooded, Cycle 11N		0.84
Per negative, flooded, Cycle 12N		0.84
Per negative, flooded, Cycle 13N		0.84

Maximum Output	Negative Electrode Discharge Rate, hours	Ampere-Hours
Per negative, flooded, Cycle 6N	2	0.582
Per negative, flooded, Cycle 7N	2	0.603
Per negative, flooded, Cycle 8N	2	0.568
Per negative, flooded, Cycle 9N	4.5	0.618
Per negative, flooded, Cycle 10N	21	0.744
Per negative, flooded, Cycle 11N	2	0.656
Per negative, flooded, Cycle 12N	45	0.719
Per negative, flooded, Cycle 13N	2	0.640
Theoretical negative capacity based on chemical analysis		0.823

(a) 91 percent of theoretical capacity.

The observed voltage-time curves for some of the cycles listed in Table 7 were plotted in Figures 12 and 13. The most striking feature of those voltage-time curves is that the single-negative-electrode voltage was essentially independent of the rate of discharge. The single-positive-electrode voltage, by contrast, depends greatly on rate of discharge, as shown in Figure 14. The constant negative-electrode voltage with changing rate of discharge is important because it implies that large pores might be used for the cadmium electrode without any increase in polarization.

Another value to be deduced from Table 7 is a conversion factor between current density and hourly rate of discharge. The negative electrodes in Table 7 have the same area dimensions as the positive electrodes described in Table 6, namely, 29.6 cm² of porous powder area on both sides. The negative electrodes of Table 7 were discharged at 320 milliamperes, as were the positive electrodes in Table 6, but required 2 hours for complete discharge because of excess negative active material relative to the active material in a positive electrode. However, in a sealed cell or battery, the hourly rate is always determined by the limiting positive capacity. Therefore, for both positive and

negative electrodes, 10.8 ma/cm^2 corresponds to a 1.5-hour rate of discharge; 16.2 ma/cm^2 corresponds to a 1.0-hour rate of discharge; and 5.4 ma/cm^2 corresponds to a 3.0-hour rate of discharge, as described earlier.

Hydrogen Effect. The discharge curves for the single negative electrode show in some cases, Cycles 6N, 10N, and 12N, Figures 12 and 13, a secondary stage reaction similar to that mentioned previously with the single positive electrode. S. Uno Falk reports that hydrogen may be adsorbed by porous metals, thus giving some extra capacity on discharge.*

This excess capacity has been eliminated from capacity measurements by using a cutoff voltage of -1.0 volt with respect to the saturated calomel reference electrode. This cutoff voltage is justified since, when no hydrogen is present, the capacity observed at a cutoff of -1.0 volt differs within a few percent of that observed at zero volt.

Current derived from adsorbed hydrogen appears only occasionally. When such current does appear, it occurs only after the majority of cadmium metal is oxidized and at a more positive voltage. Consequently, a negative cadmium electrode might be saturated with adsorbed hydrogen and that hydrogen might remain unoxidized through many cycles in a sealed cell. This follows because the cadmium is never fully oxidized in an "unbalanced" sealed cell. The hydrogen, once oxidized, does not reappear on subsequent cycles unless charging is carried to the point of considerable hydrogen evolution. Thus the charging history determines whether a hydrogen current will appear at the end of the cadmium discharge.

Cycling Effect. Although tested identically, negative plates gave smaller capacities with each cycle (see Figure 15). This result with deep cycling of negative electrodes is quite different from the reproducibility described in the section discussing the positive electrode. This loss of capacity with deep cycling of negative electrodes has been recognized by other workers** and adds another complication to the experimental work. At worst, the result means that duplicate data can be achieved only by using duplicate electrodes. At best, the result shows this project is properly directed toward a study of the single negative electrode which has a serious and fundamental weakness.

Literature concerning the loss of capacity of the negative electrode with deep cycling discloses possible causes of the effect and illustrates methods of retarding or possibly eliminating such losses. For example, the literature has many references to the use of expanders to prevent contraction of the active material in negative plates of both acid and alkaline batteries. Three basic types of expanders which have been used in the preparation of negative plates are lampblack, barium sulfate, and lignin.*** However, later work with sintered nickel electrodes has shown that the addition of indium or celulosic materials to the negative plate greatly retards capacity losses due to cycling.**

Furthermore, A. Fleischer reports that the capacity loss in the negative plate is a complex function of the discharge rate, the charging rate, and the open-circuit stand in the as-discharged state.**** It was observed that cycle losses were eliminated to a

*Falk, S. Uno, J. Electrochem. Soc., 107, 663 (1960).

**Fleischer, A., Eleventh Annual Battery Research and Development Conference, pages 83-86 (May, 1957).

***Vinal, Storage Batteries, pages 24-27.

****Fleischer, A., Tenth Annual Battery Research and Development Conference, pages 37-41 (1956).

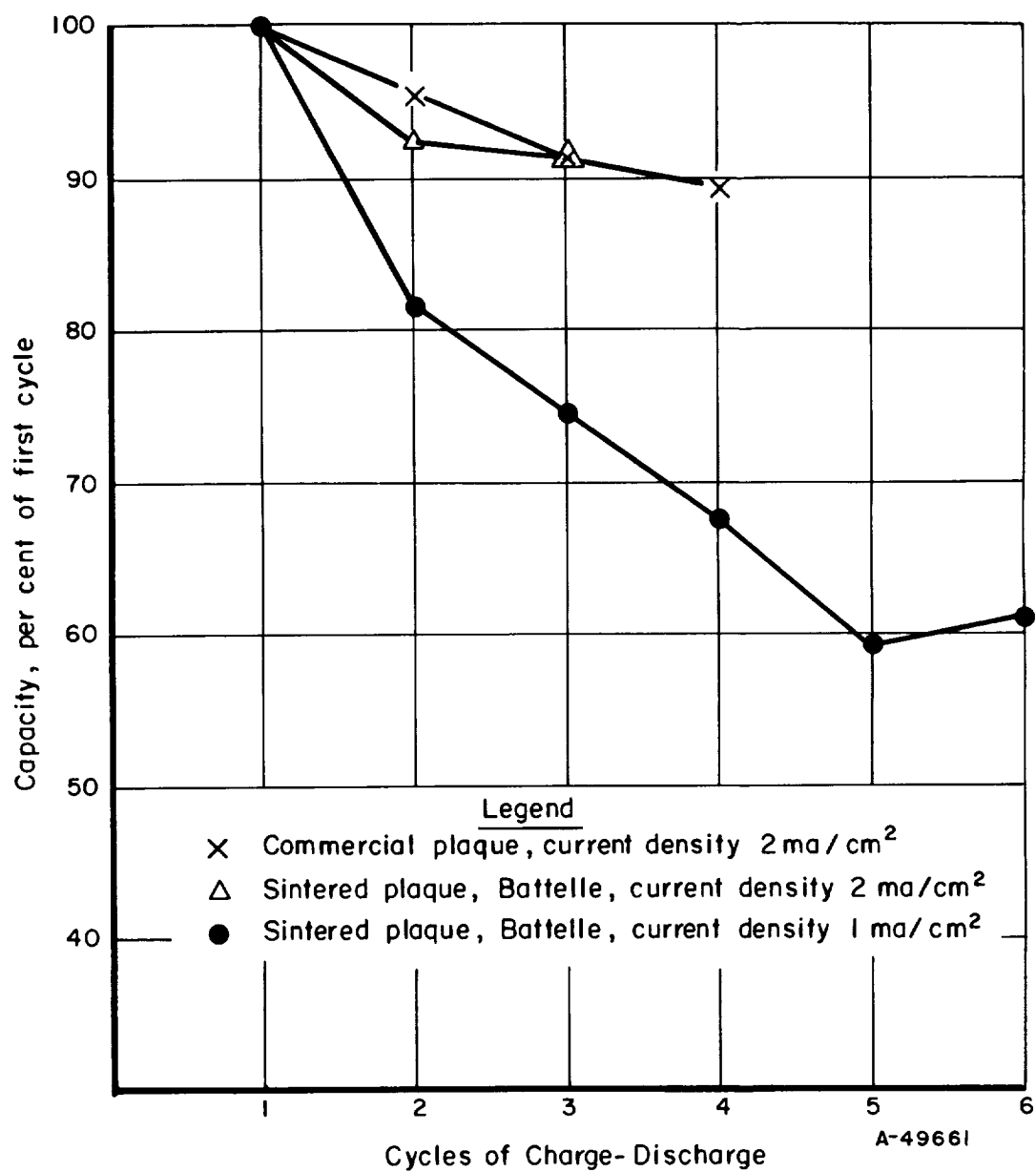


FIGURE 15. CAPACITY OF NEGATIVE PLATES AS A FUNCTION OF CHARGE-DISCHARGE CYCLES

large extent by increasing the charging-current density to 22 ma/cm² or higher as compared with conventional current densities of about 1 ma/cm². Fleischer reports that the highest rate of loss occurs when the discharge is at intermediate rates, i. e., 22 ma/cm².^{*} A current density of about 10 ma/cm² corresponds to the 2-hour rate in Figure 15.

The data in Figure 15 show the capacity loss with each cycle plotted as a percentage of the capacities obtained on the first cycle. The sintered plaque, Battelle impregnated, which was subjected to the normal charging-current density, recommended by most manufacturers, shows the greatest capacity decreases, almost 20 percent of the first cycle capacity. The sintered plaque, Battelle impregnated, which was charged at twice this current density, shows a decrease of less than 10 percent after the first cycle. This is in agreement with the literature previously cited. However, the commercial sintered nickel plaque, even though subjected to twice the normal cycling-current densities, showed the least loss in the first cycle.

At the end of the third cycle, both the commercial electrode and the Battelle impregnated plaque had the same capacity when charged at 2 ma/cm². Even though the agreement happened to be good, comparison of the commercial electrode with the Battelle impregnated plaques is difficult because the history of the commercial electrodes is unknown.

Because of the importance of capacity losses in the negative plate, a detailed analysis was undertaken to determine the effect of active-material aggregation in the sintered nickel plate. In addition, it was decided to view the effect of particle size of the active material as a variable causing capacity losses. It is reported that the capacity losses in the negative electrode are associated with the increase of the crystal size of active deposits, cadmium metal, and cadmium hydroxide on the electrode.^{**} However, according to X-ray studies, the capacity decrease on cycling is reported to be due not simply to crystal growth, defect of crystal lattice, or compound change. It is furthermore concluded that the capacity loss is mainly due to the aggregation of microparticles of cadmium.^{***}

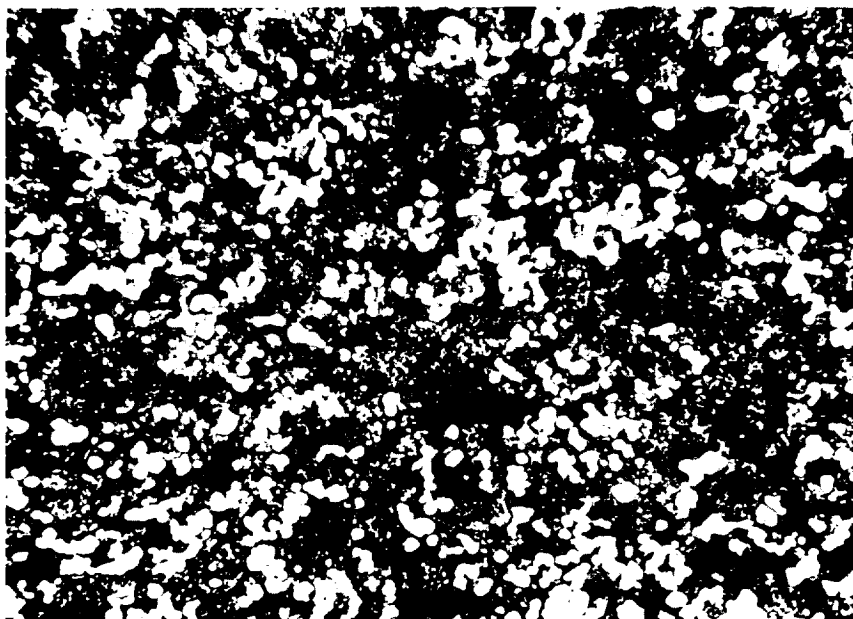
Photomicrographs were taken of cross sections of several negative plates before and after cycling. Figures 16 and 17 are photomicrographs of the same cross section of a commercial electrode in a charged condition prior to cycling. White lines were added to Figure 17 to show the outlines of several large pores in the electrode. These large pores are filled with cadmium metal, which appear as small white spots. Similar large pores (black areas) were seen in unimpregnated sintered nickel plaques, as shown in Figure 3 of the First Quarterly Progress Report.

Figures 18 and 19 are photomicrographs of cross sections of commercial and Battelle impregnated plaques after five charge-discharge cycles. The discharges were taken to 100 percent of capacity. Note that the photomicrographs show areas void of cadmium. These areas correspond to the large pores in the original nickel structure. Thus, during deep cycling of a negative electrode, the active material (cadmium) shifts position and collects in the smaller pores. This movement coincides with loss in capacity of the electrode with no loss in electrode weight. Packing of the cadmium in the smaller pores should reduce its availability for electrolytic reaction.

^{*}Fleischer, A., Eleventh Annual Battery Research and Development Conference, pages 83-86 (May, 1957).

^{**}Yamashita, D., and Yamamoto, Y., Kogyo Kagaku Zasshi, 67 (4), 536-9 (1964), Japan.

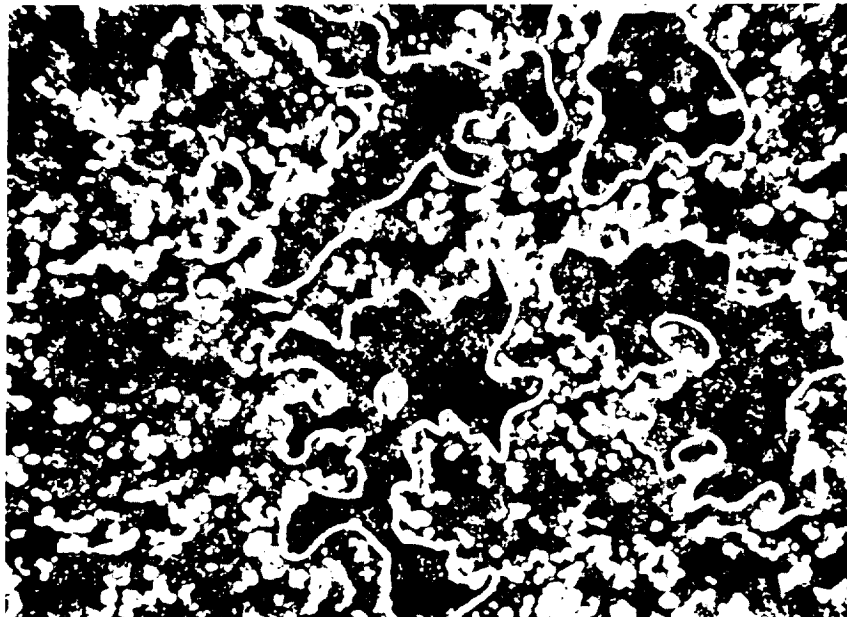
^{***}Sugita, K., Denki Kagaku, 29 (3), 176-9 (1961), Japan.



500X

17244

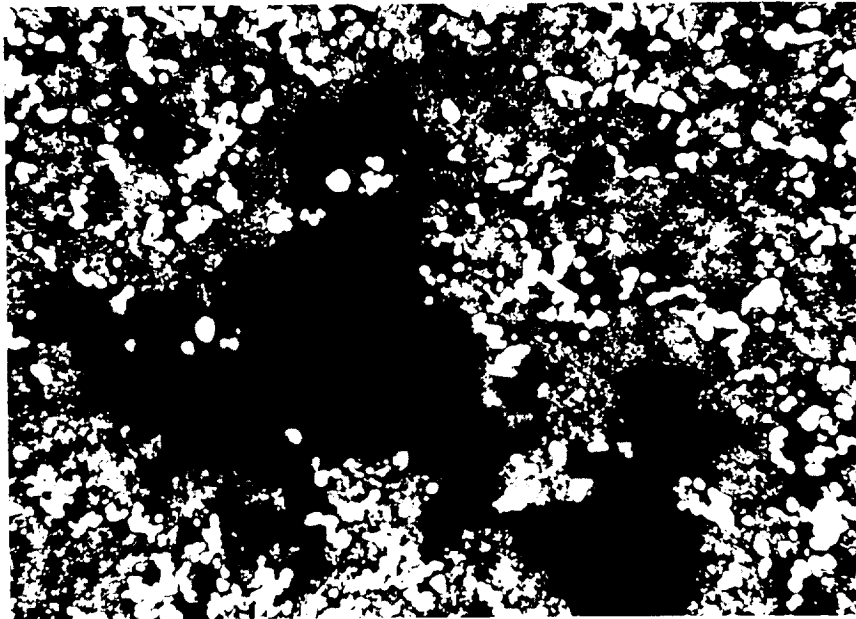
FIGURE 16. CROSS SECTION OF A COMMERCIAL IMPREGNATED BATTERY PLATE
BEFORE CYCLING (WITHOUT OVERLAY)



500X

17244

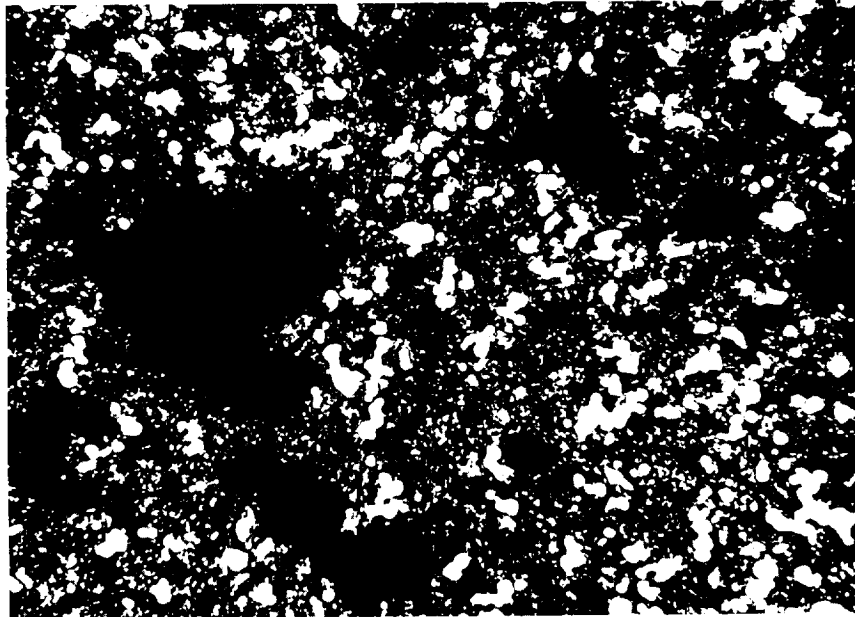
FIGURE 17. CROSS SECTION OF A COMMERCIAL IMPREGNATED BATTERY PLATE
BEFORE CYCLING (WITH OVERLAY)



500X

17245

FIGURE 18. CROSS SECTION OF A COMMERCIAL IMPREGNATED BATTERY PLATE
AFTER FIVE CHARGE-DISCHARGE CYCLES OF 100 PERCENT DEPTH



500X

17246

FIGURE 19. CROSS SECTION OF BATTELLE IMPREGNATED COMMERCIAL SINTERED
NICKEL PLATE AFTER FIVE CHARGE-DISCHARGE CYCLES OF 100
PERCENT DEPTH

So far as can be determined from review of the literature, the movements of negative material from large pores to small pores during cycling seems to be a new discovery. The result implies that uniform large pores may be preferred for best operation in a sealed battery.

N/P Ratios. The ratio of negative material to positive material (N/P ratio) is a significant parameter. Sealed nickel-cadmium batteries require an excess of negative plate capacity to avoid evolution of hydrogen. Hydrogen gas is not easily oxidized and any accumulation of the gas would tend to permanently pressurize the cell, perhaps bursting it. Excess negative material avoids the hydrogen evolution problem but adds dead weight to a battery. Therefore, the N/P ratio must be minimized to decrease the weight of batteries. The N/P ratio is used frequently in battery literature with two different bases: (1) by weight and (2) by electrochemical capacity.

The ratio is more commonly used to designate the ratio of the weight of cadmium hydroxide to weight of nickel hydroxide per unit volume of plaque. Fleisher* reports that an N/P weight ratio of 1.75 is considered normal after four chemical impregnation cycles. Sonotone Corporation considers an N/P weight ratio of 1.7 as normal in its production processing.** However, in subsequent work, Fleischer lists variations of the N/P weight ratio, after four impregnation cycles, of from 1.381 to 1.539, with an average weight ratio of 1.449.***

The commercial plaques under consideration as comparison standards show an N/P weight ratio of 1.232 based on figures obtained from Table 3, after compensating for the electrode-thickness difference between the positive and negative electrode. The weight ratios are generally of interest in connection with the impregnation process.

A more practical N/P ratio is a capacity ratio, in which N is the ampere-hours per unit volume of negative plate and P is the ampere-hours per unit volume of positive plate. An ideal capacity ratio would be $N/P = 1.0$, which would correspond to a weight ratio of $N/P = 0.79$. However, extra negative capacity is needed

- (a) To compensate for oxygen pressure within a sealed cell
- (b) To avoid less than 100 percent negative charging efficiency toward the end of charge or during overcharge, and
- (c) To compensate for loss of negative capacity by the cycling effect.

The excess negative material required to compensate for oxygen evolution at end of charge is given by****

$$\text{ampere-hours} = 4.39 \times 10^{-3} \frac{\text{amp-hr}}{\text{atm} \times \text{cm}^3} \times P \times V,$$

*Fleischer, A., J. Electrochem. Soc., 94, 296 (1948).

**Alliegro, F., and Mundel, A., Proceedings of the 15th Annual Power Sources Conference (May 9-11, 1961) p 67.

***Fleischer, A., Nickel Cadmium Battery Corporation, "Investigations on the Improvement in the Performance Characteristics of the Nickel Cadmium Battery", First Quarterly Progress Report (August 14, 1956), p 37.

****Batteries, Proceedings of the 3rd International Symposium, Bournemouth (October 1962), Edited by D. H. Collins, MacMillan Company, New York (1963), "Kinetic Basis for the Operating Characteristics of Sealed Nickel Cadmium Cells" (Upton B. Thomas, Jr.), pp 123-125.

where

P is the maximum operating pressure in the sealed cell

V is the free volume within the cell.

Assuming P is 5 atmospheres, the minimum negative plate reserve for the commercial cell of Table 3 is 0.101 amp-hr. Since the positive plates described in Table 3 had an observed capacity of 1.19 amp-hr, the negative plates must have a minimum of 1.29 amp-hr to allow for the oxygen evolution. The theoretical minimum capacity ratio is, therefore, $N/P = 1.08$.

The results in Table 7 show that not all of the impregnated cadmium hydroxide is effectively available. Efficiency varied from 90 percent to 69 percent, depending on the rate of discharge. Results on charging reported later in Table 8 also show that 10 percent of the negative material is probably untouched with normal charging procedures. Therefore, the capacity ratio should be increased at least another 10 percent, to $N/P = 1.19$, to prevent hydrogen evolution.

The loss of negative-discharge capacity with cycling, described above, should occur also with charging efficiency. This cycling loss might amount to 30 percent of the first cycle, as illustrated in Figure 15. Increasing the capacity ratio another 30 percent leads to an estimated desired value of $N/P = 1.55$. The above-mentioned N/P weight ratio of 1.232 corresponds to a capacity ratio of $N/P = 1.57$.

The net results are:

	<u>Capacity Ratios</u>	<u>Weight Ratios</u>
Ideal	1.0	0.79
Theoretical minimum for a sealed cell	1.08	0.85
Minimum for 90 percent charging efficiency	1.19	0.94
Minimum to allow for 60 percent charging efficiency after cycling	1.55	1.22
Observed, theoretical negative divided by Cycle 9P, Table 6	1.57	
Observed, Table 3		1.23
Published industrial practice ^(a)	2.15	1.7

(a) Alliegro, F., and Mundel, A., Proceedings of the 15th Annual Power Sources Conference (May 9-11, 1961), p 67.

Newly designed electrodes with straight-through and shaped pores might increase the charging efficiency and decrease cycling loss. If this hope materializes, the N/P ratios might be substantially decreased toward the theoretical minimum of a capacity N/P of 1.08 and a weight N/P of 0.85. Any improvement in N/P ratios will improve the weight and size factors of batteries.

Energy-Conversion Factors. New single experimental electrodes will be compared with single commercial electrodes in several steps:

Step 1 - Theoretical. Measure the gross dimensions of experimental electrodes and the weight of impregnated cadmium hydroxide. Calculate theoretical lb/amp-hr and in.³/amp-hr and multiply both values by 1.08, which is the theoretical minimum N/P capacity ratio. Compare the results obtained using the following equations:

$$TWI = \frac{(\text{lb/amp-hr})_{\text{comm.}} - (\text{lb/amp-hr})_{\text{Ex.}}}{(\text{lb/amp-hr})_{\text{comm.}}} \times 100$$

and

$$TVI = \frac{(\text{in.}^3/\text{amp-hr})_{\text{comm.}} - (\text{in.}^3/\text{amp-hr})_{\text{Ex.}}}{(\text{in.}^3/\text{amp-hr})_{\text{comm.}}} \times 100 ,$$

where

TWI = Theoretical weight improvement

TVI = Theoretical volume improvement

(lb/amp-hr)_{comm.} = 0.0202

(in.³/amp-hr)_{comm.} = 0.151 .

The two values, 0.0202 and 0.151, were obtained from the analytical value of 0.823 amp-hr (Table 7) contained in 0.0106 lb and 0.079 in.³ of commercial negative electrode (Table 3) after multiplication by the observed N/P capacity ratio of 1.57 given in the previous section of this report.

Step 2 - Electrochemical. Using experimental electrodes that indicate a theoretical weight and volume improvement in Step 1, measure single-electrode potentials and capacities, as a function of current density, depth of discharge, pore size, pore shape, and electrode thickness.

- (a) Using physical dimensions and the measured ampere-hours, combine the observed half-cell voltages with positive half-cell voltages from Figure 14 to calculate energy outputs as lb/whr and in.³/whr for the experimental electrode.
- (b) Note the fractional charging efficiency to hydrogen evolution for each experimental electrode and divide 1.08 by this efficiency to obtain a new N/P capacity ratio.
- (c) Multiply the new lb/whr and in.³/whr, from (a) above, by the calculated N/P capacity ratio, from (b) above, and multiply again by 3/2 to allow for an extra negative electrode in the five-electrode cell whose characteristics are given in Table 5. The results are to be

compared with Item 5 of Table 5 for a discharge current density of 10 ma/cm^2 and a charging-current density of 1 ma/cm^2 .

Step 3 - Cycle. Deep cycle electrodes from Step 2, as indicated in Figure 15 for the Battelle impregnated commercial sintered nickel powder plaques. Note any loss in ampere-hour charging efficiency after four cycles and correct the N/P capacity ratio, determined in Step 2, to obtain a final N/P capacity ratio. This final capacity ratio is obtained by dividing 1.08 by the fractional ampere-hour charging efficiency remaining after four deep cycles. Calculate the final lb/whr and $\text{in.}^3/\text{whr}$ after four deep cycles, multiply by the final N/P capacity ratio, multiply again by $3/2$, and compare the result with Item 5 in Table 5.

Step 4 - Overall. Using the best results from Step 3, total the new values in Table 5 to obtain new values for lb/whr and $\text{in.}^3/\text{whr}$ for both a cell and a battery. Invert the results to whr/lb and whr/ in.^3 and calculate improvements with the equations given on page 28 of the First Quarterly Progress Report. The commercial values, from Table 7 of the First Quarterly Progress Report, are to be used for comparison:

$$(\text{whr/lb cell})_{\text{comm.}} = 10.6, (\text{whr/in.}^3 \text{ cell})_{\text{comm.}} = 0.695$$

$$(\text{whr/lb battery})_{\text{comm.}} = 6.46, (\text{whr/in.}^3 \text{ battery})_{\text{comm.}} = 0.495$$

Experimental Screen Electrodes

The first experimental electrodes were constructed by stacking screens to a thickness of 5 mils with wires positioned in a 45-degree orientation between adjacent screens. The screen electrodes were then etched to about 60 percent porosity and impregnated with cadmium hydroxide. The method of impregnation described on page 25 in the First Quarterly Progress Report was used. The etching caused separations of the stacked screens and resulted in excessive weight gains from impregnation in some electrodes.

Electrodes were subjected to several charge-discharge cycles and the capacity losses as a function of cycle number were noted. The charging-current density used was 0.5 ma/cm^2 except for Cycle 1, in which the current density was 1.9 ma/cm^2 . All electrodes were discharged at 10 ma/cm^2 .

Effect of Pore Size. The data in Figure 20 indicate that a relationship exists between pore size and loss of capacity on cycling in the experimental screen electrodes. The percent capacity is plotted as a function of cycle number, Figure 20, with the capacity obtained in Cycle 1 considered as 100 percent. The electrodes with the larger pores retain more capacity upon cycling than electrodes with smaller pores. Pore sizes are given on pages 7 and 9 of the First Quarterly Progress Report. However, since the data shown in the tables are for electrodes with straight-through pores, pore sizes in electrodes with 45-degree orientation will be comparatively smaller.

The curve for the Battelle impregnated commercial sintered nickel plaque closely follows the curve for the 1000 lines/inch screen electrode. Both electrodes have average pore diameters of about the same order of magnitude (0.6 mil), and such a

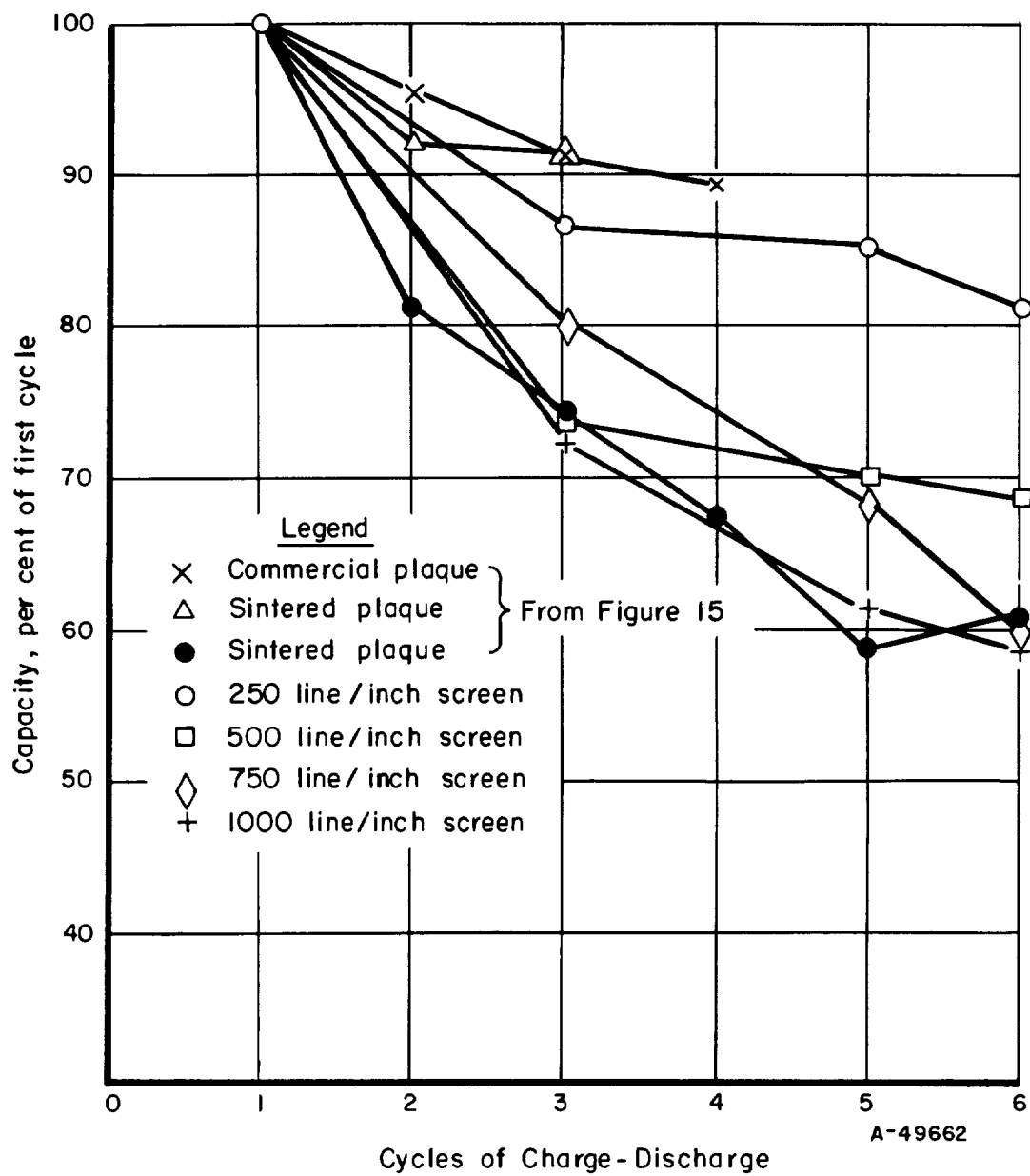


FIGURE 20. CAPACITY OF NEGATIVE PLATES AS A FUNCTION OF CHARGE-DISCHARGE CYCLES

relationship would be expected. The results from the limited data obtained on experimental screen electrodes is encouraging, especially considering that straight-through holes will result in larger pore diameters and should give better performance than that observed with the 45 degree orientation.

Energy Input

Commercial Standard Electrodes

Standard electrodes were prepared and tested as described in Evaluation Method under Item I. However, a different electrode was used in each test due to the loss of capacity, which occurs on cycling, of the negative plate discussed earlier under cycle effects. Prior to testing, the electrodes were in the completely discharged condition. The electrodes were charged at various rates and then discharged all at the same rate for comparison. The whr/lb and whr/in.³ were calculated from the experimental results (see Table 8).

TABLE 8. ENERGY-OUTPUT DENSITIES AS A FUNCTION OF CHARGING-CURRENT DENSITY AFTER 30 PERCENT OVERCHARGE

Charging- Current Density, ma/cm ²	Input to H ₂ Evolution, amp-hr x 10 ²	Output, amp-hr x 10 ²	Output, whr x 10 ²	Electrode Weight, lb x 10 ⁴	Energy Output Densities	
					Whr Lb	Whr In. ³
96.5	2.89	3.74	4.53	6.75	67.1	9.27
48.0	2.64	3.98	4.83	6.87	70.3	9.90
24.0	4.24	4.01	4.87	7.00	69.6	9.99
9.64	4.72	3.84	4.66	6.85	68.0	9.56
4.8	4.72	3.71	4.50	6.85	65.7	9.22
2.4	4.95	3.52	4.27	6.75	63.3	8.76
2.4	5.11	3.72	4.51	6.96	64.8	9.24
0.5	--	4.00	4.85	7.08	68.5	9.95

Effects of Current Density. The standard electrodes were charged for 130 percent of theoretical capacity to note the effect of overcharge. Experimental results indicate that the 30 percent overcharge was sufficient to completely charge each electrode since all outputs were similar. The average charge efficiency is greater than 60 percent during the portion of the charge curve when hydrogen is evolved even at the highest current density used. All charging curves were recorded. A typical charging curve is shown in Figure 21. The ampere-hours were determined for the two portions of the charge curve, i. e., from start of charging to hydrogen evolution and from hydrogen evolution to the end of charge by use of the inflection of the voltage-time curves during the charge as the separation point. The data in Table 8 show the definite relationship between charging-current density and charge efficiency. The input coulombs required to evolve hydrogen at the negative electrode are inversely proportional to the charging-current density. Extrapolation of results to zero current density in Figure 22 shows that charging

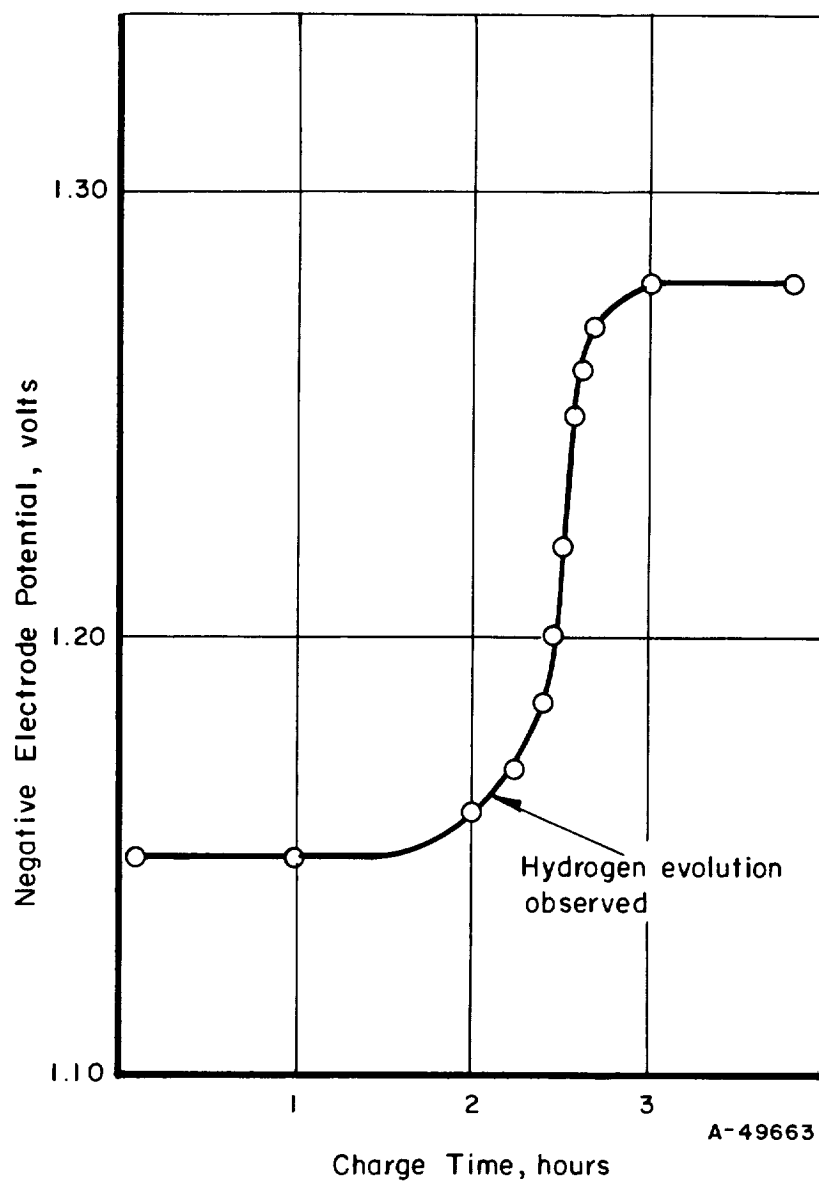


FIGURE 21. CHARGE CURVE FOR NEGATIVE ELECTRODE AT A CURRENT DENSITY OF 9.65 MA/CM^2

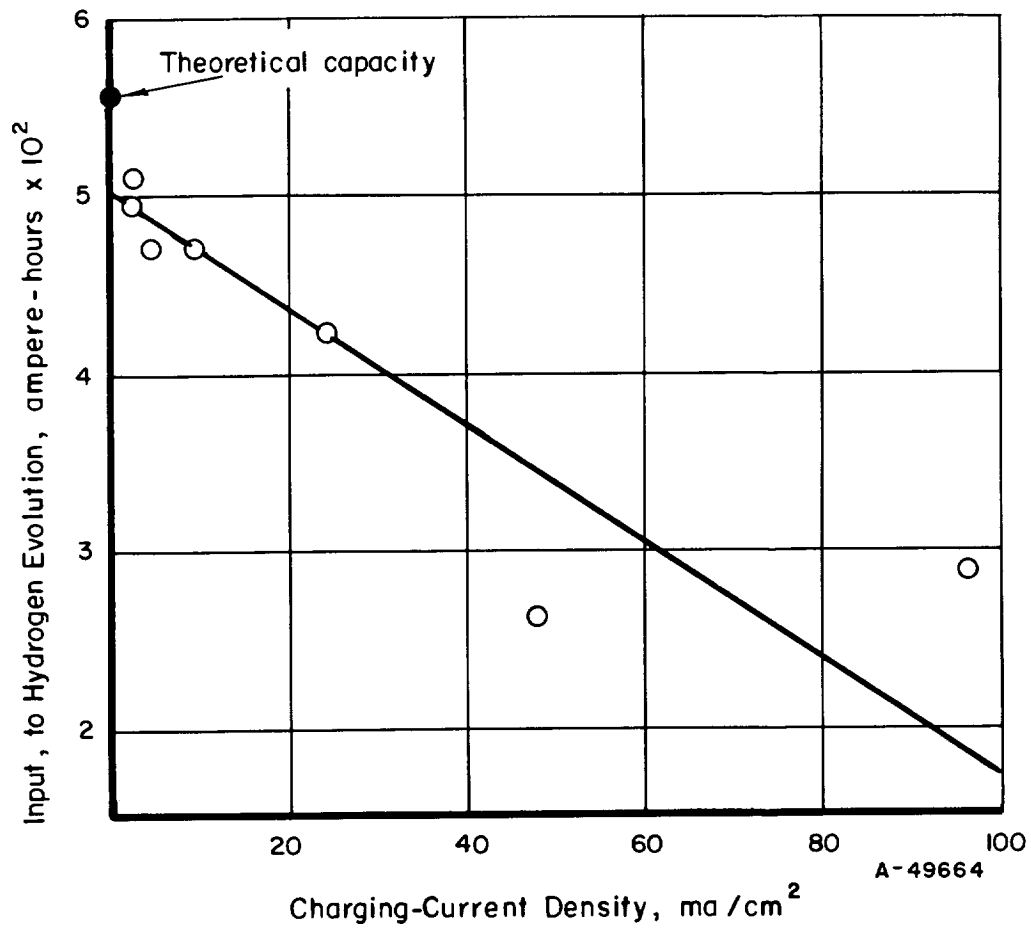


FIGURE 22. COULOMBIC INPUT TO EVOLVE HYDROGEN AS A FUNCTION OF CHARGING-CURRENT DENSITY

efficiency is always less than 90 percent. Therefore, a sealed cell with these electrodes must have an additional 10 percent excess negative material to avoid hydrogen evolution. In Table 8, the following values were constant for each current density.

Average theoretical capacity	0.0556 amp-hr
Total input	0.0723 amp-hr
Discharge-current density	24 ma/cm ²
Average negative voltage	1.11 volts
Calculated cell voltage	1.212 volts
(From Figure 14)	

The value at 2.4 ma/cm² was repeated as a checkpoint.

In summary, the data presented have clearly indicated that the optimum end point in the charging cycle must be taken at the first indication of hydrogen evolution. Only then can meaningful results be obtained from input data which will be applicable to a sealed cell.

Future Work

Commence testing of experimental stacked screen electrodes prepared under Task B that have successfully passed the requirements previously set in Step 1, Energy Conversion Factors, in the Second Quarterly Progress Report.

Location of Data

All experimental data on Task F are contained in Battelle Laboratory Record Book No. 21685, pages 9-74.

JM/GRS/DGT/CLF:pa

DISTRIBUTION LIST

National Aeronautics & Space Administration
Washington, D. C. 20546
Attention: Ernst M. Cohn, Code RNW
James R. Miles, Code SL
A. M. Andrus, Code ST

National Aeronautics & Space Administration
Scientific and Technical Information Facility
P. O. Box 5700
Bethesda, Maryland, 20014 (3)

National Aeronautics & Space Administration
Ames Research Center
Moffett Field, California
Attention: A. S. Hertzog/J. R. Swain

National Aeronautics & Space Administration
Goddard Space Flight Center
Greenbelt, Maryland
Attention: Thomas Hennigan, Code 636

National Aeronautics & Space Administration
Langley Research Center
Langley Station
Hampton, Virginia
Attention: S. T. Peterson
John L. Patterson, MS 234

National Aeronautics & Space Administration
Lewis Research Center
21000 Brookpark Road
Cleveland, Ohio 44135
Attention: R. R. Miller, MS 500-202
N. D. Sanders, MS 302-1
Robert L. Cummings, MS 500-201
Library
B. Lubarsky, MS 500-201
J. E. Dilley, MS 500-309
J. J. Weber, MS 3-16
M. J. Saari, MS 500-202
W. A. Robertson, MS 500-201 (1 copy + 1 repro.)

National Aeronautics & Space Administration
Manned Spacecraft Center
Houston 1, Texas
Attention: Robert Cohen - Gemini Project Office
Richard Ferguson (EP-5)
James T. Kennedy
F. E. Eastman (EE-4)

National Aeronautics & Space Administration
Marshall Space Flight Center
Huntsville, Alabama
Attention: Philip Youngblood

Jet Propulsion Laboratory
4800 Oak Grove Drive
Pasadena, California
Attention: Aiji Uchiyama

U. S. Army Engineer R&D Labs.
Fort Belvoir, Virginia
Attention: Electrical Power Branch

U. S. Army Engineer R&D Labs.
Fort Monmouth, New Jersey
Attention: Arthur F. Daniel (Code SELRA/SL-PS)
David Linden (Code SELRA/SL-PS)

Harry Diamond Labs.
Room 300, Building 92
Connecticut Avenue & Van Ness Street, N.W.
Washington, D. C.
Attention: Nathan Kaplan

Army Materiel Command
Research Division
AMCRD-RSCM T-7
Washington 25, D. C.
Attention: John W. Crellin

U. S. Army TREGOM
Physical Sciences Group
Fort Eustis, Virginia
Attention: (SMOFE)

U. S. Army Research Office
Box CM, Duke Station
Durham, North Carolina
Attention: Dr. Wilhelm Jorgensen

U. S. Army Mobility Command
Research Division
Center Line, Michigan
Attention: O. Renius (AMSMO-RR)

Hq., U. S. Army Materiel Command
Development Division
Washington 25, D. C.
Attention: Marshall D. Aiken (AMCRD-DE-MO-P)

Office of Naval Research
Department of the Navy
Washington 25, D. C.
Attention: Dr. Ralph Roberts

Bureau of Naval Weapons
Department of the Navy
Washington 25, D. C.
Attention: (Code RAAE)

Naval Ammunition Depot
Crane, Indiana
Attention: E. Bruess

Bureau of Ships
Department of the Navy
Washington 25, D. C.
Attention: Bernard B. Rosenbaum (Code 340)
C. F. Viglotti (Code 660)

Naval Ordnance Laboratory
Department of the Navy
Corona, California
Attention: Mr. William C. Spindler (Code 441)

Naval Ordnance Laboratory
Department of the Navy
Silver Spring, Maryland
Attention: Philip B. Cole (Code WB)

U. S. Naval Research Laboratory
Washington, D. C. 20390
Attention: Code 6160

Wright-Patterson AFB
Aeronautical Systems Division
Dayton, Ohio
Attention: J. E. Cooper

AF Cambridge Lab.
L. G. Hanscom Field
Bedford, Massachusetts
Attention: Francis X. Doherty

Rome Air Development Center, ESD
Griffiss AFB, New York
Attention: Frank J. Mollura (RASSM)

Office of the Deputy Commander AFSC
for Aerospace Systems
United States Air Force
Los Angeles 45, California
Attention: W. J. Bennison

Mr. Donald B. Hoatson
Army Reactors, DRD
U. S. Atomic Energy Commission
Washington 25, D. C.

Defense Documentation Center Headquarters
Cameron Station, Building 5
5010 Duke Street
Alexandria 4, Virginia
Attention: TISIA

Institute for Defense Analyses
1666 Connecticut Avenue, N. W.
Washington 9, D. C.
Attention: Dr. G. Szego

National Bureau of Standards
Washington 25, D. C.
Attention: Dr. W. J. Hamer

Power Information Center
University of Pennsylvania
Moore School Building
200 South 33rd Street
Philadelphia 4, Pennsylvania

Office of Technical Services
Department of Commerce
Washington, D. C. 20009

Mr. R. A. Eades
D.R.S.
British Embassy
3100 Massachusetts Avenue, N.W.
Washington 8, D. C.

Canadian Joint Staff
Defense Research Member (WASA)
2450 Massachusetts Avenue, N. W.
Washington 25, D. C.

Power Sources Division
Whittaker Corporation
P. O. Box 337
Newbury Park, California
Attention: J. Rhyne

Aerospace Corporation
P. O. Box 95085
Los Angeles 45, California
Attention: Library

Allis-Chalmers Manufacturing Company
1100 South 70th Street
Milwaukee 1, Wisconsin
Attention: Dr. T. G. Kirkland

Atomics International
North American Aviation
Canoga Park, California
Attention: Dr. H. L. Recht

Battelle Memorial Institute
505 King Avenue
Columbus 1, Ohio
Attention: Dr. C. L. Faust

Buckbee Mears Company
Park Square Building
St. Paul, Minnesota 55101
Attention: Norman C. Mears

Burgess Battery Company
Freeport, Illinois
Attention: Dr. Howard J. Strauss

Clevite Corporation
Aerospace Research Division
540 East 105th Street
Cleveland, Ohio
Attention: A. D. Schwope

Delco Remy Division
General Motors Corporation
Anderson, Indiana
Attention: Dr. J. J. Lander

Dynatech Corporation
17 Tudor Street
Cambridge 34, Massachusetts
Attention: W. W. Welsh

Eagle-Picher Company
P. O. Box 290
Joplin, Missouri
Attention: E. M. Morse

Electric Storage Battery Company
Missile Battery Division
Raleigh, North Carolina
Attention: A. Chreitzberg

Electrochimica Corporation
1140 O'Brien Drive
Menlo Park, California
Attention: Dr. Morris Eisenberg

Electro-Optical Systems, Incorporated
300 N. Halstead
Pasadena, California
Attention: H. R. Erwin

Emhart Manufacturing Company
Box 1620
Hartford, Connecticut
Attention: Dr. W. P. Codogan

Federal-Mogul Division
20700 Mound Road
Warren, Michigan 48090
Attention: A. Beebe

Dr. Arthur Fleischer
466 South Center Street
Orange, New Jersey

General Electric Company
Battery Products Section
P. O. Box 114
Gainesville, Florida

General Electric Corporation
Schenectady, New York
Attention: Dr. William Carson, ATL

Globe Union Incorporated
900 East Keefe Avenue
Milwaukee, Wisconsin
Attention: Dr. C. K. Morehouse

Gould-National Batteries, Incorporated
Engineering and Research Center
2630 University Avenue, S. E.
Minneapolis 14, Minnesota
Attention: J. F. Donahue

Gulton Industries
Alkaline Battery Division
Metuchen, New Jersey
Attention: Dr. Robert Shair

Huyck Metals Department
P. O. Box 30
Milford, Connecticut
Attention: J. T. Fisher

IIT Research Institute
10 West 35th Street
Chicago 16, Illinois
Attention: Dr. H. T. Francis

Leesona Moos Laboratories
Lake Success Park, Community Drive
Great Neck, New York 11021
Attention: Dr. H. Oswin

Livingston Electronic Corporation
Route 309
Montgomeryville, Pennsylvania
Attention: William F. Meyers

Lockheed Missiles & Space Company
Sunnyvale, California
Attention: Dr. J. E. Chilton, Dept. 52-30

P. R. Mallory & Company
Technical Services Laboratories
Indianapolis 6, Indiana
Attention: A. S. Doty

P. R. Mallory & Company
Northwest Industrial Park
Burlington, Massachusetts
Attention: Dr. Per Bro

Material Research Corporation
Orangeburg, New York
Attention: V. E. Adler

Melpar, Incorporated
3000 Arlington Boulevard
Falls Church, Virginia
Attention: Dr. R. T. Foley

Monsanto Research Corporation
Everett 49, Massachusetts
Attention: Dr. J. O. Smith

Radiation Applications Incorporated
36-40 37th Street
Long Island City 1, New York
Attention: Munroe F. Pofcher

Rocketdyne Division
North American Aviation
6633 Canoga Avenue
Canoga Park, California
Attention: Dr. R. P. Frohmborg,
Department 591

Sonotone Corporation
Saw Mill River Road
Elmsford, New York
Attention: A. Mundel

Space Technology Laboratories, Incorporated
2400 E. ElSegundo Boulevard
ElSegundo, California
Attention: Dr. A. Krausz

Metals & Controls Division
Texas Instruments, Incorporated
34 Forest Street
Attleboro, Massachusetts
Attention: Dr. E. M. Jost

Thompson Ramo Wooldridge, Incorporated
23555 Euclid Avenue
Cleveland, Ohio
Attention: Librarian

Union Carbide Corporation
Parma Research Center
Box 6116
Cleveland, Ohio
Attention: Meredith Wright

Westinghouse Electric Corporation
Research & Development Center
Churchill Borough
Pittsburgh, Pennsylvania
Attention: Dr. A. Langer

Yardney Electric Corporation
New York, New York
Attention: Dr. Paul Howard